

Dirichlet-tree multinomial mixtures for clustering microbiome compositions

Jialiang Mao Li Ma

Duke University, Durham, NC

October 26, 2021

Abstract

A common routine in microbiome research is to identify reproducible patterns in the population through unsupervised clustering of samples. To this end, we introduce Dirichlet-tree multinomial mixtures (DTMM) as a generative model for the amplicon sequencing data in microbiome studies. DTMM models the microbiome population with Dirichlet process mixtures to learn a clustering structure. For the mixing kernels, DTMM directly utilizes a phylogenetic tree to perform a tree-based decomposition of the Dirichlet distribution. Through this decomposition, DTMM offers a flexible covariance structure to capture the large within-cluster variations, while providing a way of borrowing information among samples in different clusters to accurately learn the common part of the clusters. We perform extensive simulation studies to evaluate the performance of DTMM and compare it to several model-based and distance-based clustering methods in the microbiome context. Finally, we analyze a specific version of the fecal data in the American Gut project to identify underlying clusters of the microbiota of IBD and diabetes patients. Our analysis shows that (i) clusters in the human gut microbiome are generally determined by a large number of OTUs jointly in a sophisticated manner; (ii) OTUs from genera *Bacteroides*, *Prevotella* and *Ruminococcus* are typically among the important OTUs in identifying clusters; (iii) the number of clusters and the OTUs that characterize each cluster can differ across different patient groups.

1 Introduction

The microbiome is the collective genomes of all microbes that inhabit a specific environment, be it an animal, a plant, or a tissue. In particular, the human microbiome is considered as a counterpart or an extension to the human genome (Grice and Segre, 2012), containing 100-fold more unique genes than the latter (Qin et al., 2010). The human microbiome has significant influences on various aspects of our physiology (Turnbaugh et al., 2009; Qin et al., 2012; Karlsson et al., 2013) and is suggested as a way towards precision medicine (Kuntz and Gilbert, 2017). The development of next-generation sequencing strategies enables us to profile the microbiome fast and economically, through either amplicon sequencing on target genes (usually the 16S ribosomal RNA gene) or shotgun sequencing on the entire microbial genome. In this work, we focus on datasets obtained from amplicon sequencing studies. Traditionally, the sequencing reads are sent to preprocessing pipelines such as QIIME (Caporaso et al., 2010) to construct clusters named operational taxonomic units (OTUs) based on certain predefined similarity threshold (typically 97%). In contrast, more recently developed pipelines such as DADA2 (Callahan et al., 2016) directly resolve amplicon sequence variants (ASVs), which is shown to outperform OTUs in terms of accuracy and interpretability (Callahan et al., 2017). OTUs and ASVs serve as the unit for the downstream analyses and provide the same interface: each sample is a vector of counts on a list of units (OTUs or ASVs), representing the composition of the underlying community. The methodology developed in this work applies to both OTUs and ASVs, we thus use the customary “OTU” to refer to the unit.

Typical tasks of microbiome research include characterizing the microbiome composition of an individual and study its relationship with various covariates, such as the host’s dietary patterns or disease status. Due to the considerable variability of human microbiome compositions, it is hard to complete these tasks directly at the individual level (Ding and Schloss, 2014). A popular way to overcome this difficulty is to first group individual samples into clusters and perform downstream analyses at the cluster level. For example, in the context of the human gut microbiome, these clusters are referred to as “enterotypes” (Arumugam et al., 2011; Costea et al., 2018), which are shown to be associated with long-term dietary habits, obesity, and Crohn’s disease (Wu et al., 2011; Holmes et al., 2012; Quince et al., 2013). Nevertheless, clustering microbiome samples is challenging. Off-the-shelf machine learning algorithms such as k -means, Partitioning Around Medoids (PAM) and hierarchical clustering that are distance-based are not satisfactory when applied to microbiome data. To get a partition of the samples into clusters, these methods entail a predetermined number of clusters or cut-offs, which is typically hard to specify in microbiome settings. In addition, popular distance metrics for microbiome compositional data such as the Bray-Curtis dissimilarity and the Unifrac distances (Lozupone and Knight, 2005) can induce improper weights to different OTUs while clustering. Koren et al. (2013) show that different methodologies to select the number of clusters can yield inconsistent clustering results and that these algorithms are sensitive to the distance metrics chosen.

Alternatively, one can achieve clustering through building a probabilistic model for the microbiome count data with a latent grouping structure, such as the mixture model. The

key to this thread is a good generative model for the OTU counts: firstly, the model needs to be flexible enough to capture the idiosyncrasy of each cluster and allow the complex variations of samples therein; secondly, it should borrow information across all samples to accurately infer the shared portion of all clusters; moreover, since biological information of the OTUs is available, it is desirable for the model to incorporate such information. By far, the most popular model-based clustering method designed for microbiome data is Dirichlet multinomial mixtures (DMM) (Holmes et al., 2012), which adopts a multinomial sampling scheme and generates the sample-specific multinomial parameters from a finite mixture of Dirichlet distributions. Unfortunately, DMM does not satisfy the above desiderata.

We illustrate some limitations of DMM with a simple example with six OTUs. Suppose that the microbiome population has three equal sized clusters. We first assume DMM is the true data generating process and denote the three Dirichlet components as $\text{Dir}(\boldsymbol{\alpha}_k)$, $k = 1, 2, 3$. Let $\boldsymbol{\alpha}_1 = (10, 2, 4, 4, 2, 2) \cdot \alpha_0$, $\boldsymbol{\alpha}_2 = (6, 6, 4, 4, 2, 2) \cdot \alpha_0$, $\boldsymbol{\alpha}_3 = (2, 10, 4, 4, 2, 2) \cdot \alpha_0$, respectively. Figure 1 (a) and (c) show the 2.5% and 97.5% percentiles of the marginals of $\text{Dir}(\boldsymbol{\alpha}_k)$ for $\alpha_0 = 10$ and $\alpha_0 = 0.25$, $k = 1, 2, 3$. Note that the single parameter α_0 governs the dispersion level of all the categories simultaneously. Therefore, although the Dirichlet distribution is flexible in capturing each cluster centroid, it is restrictive in modeling the systematic variations among samples in the same cluster around the centroid. Consequently, when DMM is applied to data with true marginals on the multinomial parameters as shown in Figure 1 (b), where different categories have different levels of dispersions, α_0 has to be estimated small to accommodate to the large dispersion of the last 4 categories, essentially washing away the strong signals contained in the first 2 categories and pooling all the samples to the same cluster. Unfortunately, this situation is not uncommon for microbiome data. In this example, the clusters are only different in the compositions of OTU 1 and 2. However, DMM ignores this common feature across clusters and overfits the data by introducing cluster-specific parameters for the compositions of the last 4 OTUs. This problem is amplified in real microbiome applications, where the number of OTUs is typically large and the overfitting can be severe when the clustering is relevant to only a portion of OTUs. Moreover, the Dirichlet distribution implies independence among OTU compositions up to the sum to one constraint (Aitchison, 1982), which is restrictive in the microbiome context (Wang and Zhao, 2017).

In this work, we propose a method, called Dirichlet-tree multinomial mixtures (DTMM), that performs model-based clustering of the microbial compositional data. Similar to DMM, our method applies the mixture model to achieve clustering under the Bayesian inference framework. Unlike DMM, we consider a more flexible mixing kernel than the Dirichlet distribution that (i) provides a more flexible covariance structure among OTU counts within a cluster and (ii) offers a solution to identify and efficiently infer the common parts across clusters. By directly bringing in a phylogenetic tree of the OTUs that summarizes their evolutionary relationship, DTMM adopts the Dirichlet-tree distribution (DT) (Dennis III, 1991) as the mixture component that sequentially generates the multinomial parameters through a series of beta distributions at the internal nodes of the phylogenetic tree. On one hand, DT introduces a set of dispersion parameters through these beta distributions that

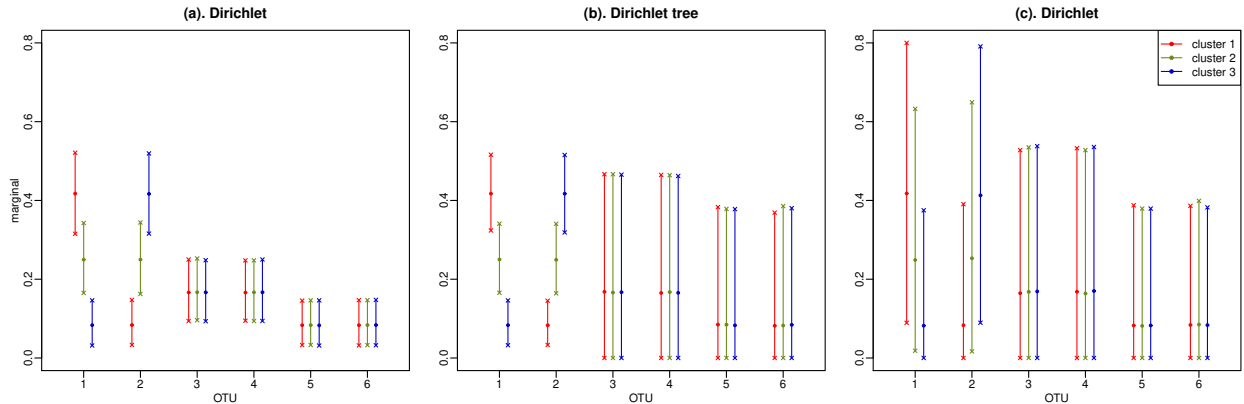


Figure 1: 2.5% and 97.5% percentiles of the marginals for each category (plots are obtained based on simulation). (a): the truth is the Dirichlet distribution, with small dispersion; (b): the truth is the Dirichlet-tree distribution (introduced in [Section 2](#)); (c): the truth is the Dirichlet distribution, with large dispersion.

allow different variation levels among the OTUs, offering a more flexible covariance structure than the Dirichlet distribution. [Figure 1](#) (b) gives an example of the marginals generated from three DT under a specific tree. On the other hand, through allowing some of these beta distributions to be shared across clusters, cluster-specific parameters are only introduced when necessary and the common portion of the clusters can be inferred accurately.

Using phylogenetic information to guide inference is a popular direction in recent microbiome research. For example, [Wang and Zhao \(2017\)](#), [Tang et al. \(2018\)](#) and [Mao et al. \(2020\)](#) use a similar DT-multinomial framework in various model-based microbiome analyses. [Silverman et al. \(2017\)](#) propose a phylogenetic-based log-ratio transform on the compositional data to a space where classical statistical tools can be applied. Other than the Dirichlet-based models, log-ratio based models such as the logistic-normal model ([Atchison and Shen, 1980](#)) are also frequently used in microbiome studies (see for example [Xia et al. \(2013\)](#) and [Li et al. \(2018\)](#)). Although offering a more flexible covariance structure than the Dirichlet distribution, these models incur challenges in inferring the high-dimensional covariance structure. As we shall see, the DT model strikes a balance between the simple but restrictive Dirichlet model and the more flexible log-ratio based models: in addition to the aforementioned modeling benefits, the tree-based decomposition allows a divide-and-conquer strategy to perform inference, in a way similar to the posterior inference of Pólya tree type models in the Bayesian nonparametric literature ([Lavine et al., 1992, 1994](#)). Instead of having to resort to optimization techniques to do inference as in DMM, fully Bayesian inference becomes practical.

The rest of the paper is organized as follows. [Section 2](#) introduces a phylogenetic tree-based decomposition of the multinomial counts and proposes DTMM for clustering OTU counts based on this decomposition. [Section 3](#) performs a series of representative numerical experiments to evaluate the performance of DTMM and validate the resulting clusters. [Sec-](#)

tion 4 applies DTMM to a specific dataset from the American Gut project to find enterotypes of samples that are diagnosed with IBD or diabetes. Section 5 concludes.

2 Method

2.1 DM and DMM

Consider a microbiome dataset with OTU counts of n samples $\mathbf{y}_1, \mathbf{y}_2, \dots, \mathbf{y}_n$. Each sample is a vector of counts of the M OTUs in the study denoted by $\Omega = \{\text{OTU}_1, \text{OTU}_2, \dots, \text{OTU}_M\} = \{\omega_1, \omega_2, \dots, \omega_M\}$. Let the i -th sample and the total counts in that sample be $\mathbf{y}_i = (y_{i1}, y_{i2}, \dots, y_{iM})$ and $N_i = \sum_{j=1}^M y_{ij}$, where y_{ij} is the count of OTU j . The samples can be stacked into an OTU table denoted by \mathbf{Y} , as shown in Table 5. In this work, we shall treat the total counts N_i 's as given since they are artificial quantities that depend on the sequencing depth rather than reflecting the true abundance of the OTUs in the sampled environment. This leads to the generative Dirichlet-multinomial model (DM) that takes the multinomial sampling scheme coupled with a Dirichlet prior on the multinomial parameters (Knights et al., 2011; La Rosa et al., 2012):

$$\begin{aligned} \mathbf{y}_i | N_i, \mathbf{p}_i &\stackrel{\text{ind}}{\sim} \text{Multi}(N_i, \mathbf{p}_i) \\ \mathbf{p}_i | \boldsymbol{\alpha} &\stackrel{\text{iid}}{\sim} \text{Dir}(\boldsymbol{\alpha}), \end{aligned} \quad (2.1)$$

where $\mathbf{p}_i = (p_{i1}, p_{i2}, \dots, p_{iM})$, p_{ij} is the probability that a count in sample i belongs to OTU j , $\boldsymbol{\alpha} = (\alpha_1, \alpha_2, \dots, \alpha_M)$ with $\alpha_j > 0$ for $j = 1, \dots, M$.

Viewing each sample as randomly drawn from an underlying ‘‘community’’ characterized by its multinomial parameter (Holmes et al., 2012), DM models all the ‘‘communities’’ as realizations of a single ‘‘metacommunity’’ governed by $\boldsymbol{\alpha}$. Holmes et al. (2012) extend DM to Dirichlet multinomial mixtures (DMM) by replacing the single Dirichlet prior in DM by a finite mixture of K Dirichlets to allow clustering of the samples into different ‘‘metacommunities’’:

$$\begin{aligned} \mathbf{y}_i | N_i, \mathbf{p}_i &\stackrel{\text{ind}}{\sim} \text{Multi}(N_i, \mathbf{p}_i) \\ \mathbf{p}_i | \boldsymbol{\pi}, \boldsymbol{\alpha}_1, \dots, \boldsymbol{\alpha}_K &\stackrel{\text{iid}}{\sim} \sum_{k=1}^K \pi_k \text{Dir}(\boldsymbol{\alpha}_k) \\ \boldsymbol{\pi} = (\pi_1, \dots, \pi_K) &\sim \text{Dir}(\mathbf{b}_0), \end{aligned} \quad (2.2)$$

where $\boldsymbol{\alpha}_k = (\alpha_{k1}, \alpha_{k2}, \dots, \alpha_{kM})$, $\boldsymbol{\pi}$ the weights of the ‘‘metacommunities’’ with $\sum_{k=1}^K \pi_k = 1$, $\pi_k \geq 0$ for $k = 1, \dots, K$. In DMM, each sample is viewed as a draw from a unique ‘‘community’’ that is itself drawn from one of the K ‘‘metacommunities’’.

As a clustering method, DMM has several limitations. Most importantly, it could not adequately model the within cluster variation of the microbial composition. This can be seen by writing the cluster-specific Dirichlet parameter $\boldsymbol{\alpha}_k$ as $\boldsymbol{\alpha}_k = \alpha_{k0} \cdot \bar{\boldsymbol{\alpha}}_k$, where $\bar{\boldsymbol{\alpha}}_k$ lying in the $(M - 1)$ -dimensional simplex represents the prior mean of the multinomial probabilities in cluster k , $\alpha_{k0} = \sum_{j=1}^M \alpha_j$ determines the within cluster variation of all these probabilities around $\bar{\boldsymbol{\alpha}}_k$ simultaneously. Secondly, the multinomial parameters in DM are modeled

independently up to the sum to one constraint (Mosimann, 1962), which is not suitable in the microbiome context since the OTUs are functionally and evolutionarily related. Moreover, although DMM is specified within the Bayesian framework, the posterior inference is performed by optimization through an EM algorithm with Laplace approximations of the marginal likelihoods. When the number of OTUs is moderate, which is typical in microbiome studies, these techniques are numerically unstable and cannot provide reliable uncertainty quantifications.

| Sample | ω_1 | ω_2 | \cdots | ω_M | Sum |
|----------|------------|------------|----------|------------|----------|
| 1 | y_{11} | y_{12} | \cdots | y_{1M} | N_1 |
| 2 | y_{21} | y_{22} | \cdots | y_{2M} | N_2 |
| \vdots | \vdots | \vdots | \ddots | \vdots | \vdots |
| n | y_{n1} | y_{n2} | \cdots | y_{nM} | N_n |

Table 1: An $n \times M$ OTU table.

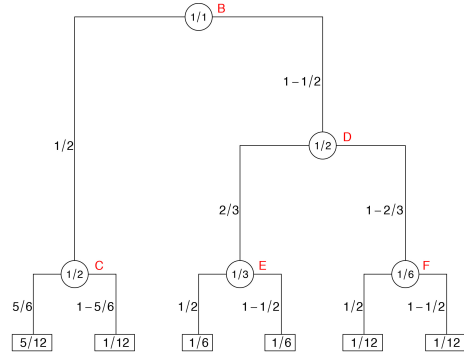


Figure 2: A tree based generation of \mathbf{p}_{ex} .

2.2 Dirichlet-tree multinomial mixtures

A key feature of microbiome count data is that the categories (OTUs) are functionally and evolutionarily related. Typically, this relationship can be summarized into a rooted phylogenetic tree. In this phylogenetic tree, each internal node can be viewed as a “taxa” that represents the most recent common ancestor of its descendant OTUs. Let $\mathcal{T} = \mathcal{T}(\mathcal{I}, \mathcal{U}; \mathcal{E})$ be a rooted full binary phylogenetic tree over the M OTUs in the study, where \mathcal{I} , \mathcal{U} and \mathcal{E} denote the set of internal nodes, leaves and edges of \mathcal{T} , respectively. We denote each node $A \in \mathcal{I} \cup \mathcal{U}$ by the set of its descendant OTUs. In particular, $A = \Omega$ denotes the root of \mathcal{T} ; $A = \{\omega_j\}$ represents the leaf that contains OTU j for $j = 1, \dots, M$. With our notation, $\mathcal{U} = \{\{\omega\} : \omega \in \Omega\}$. For $A \in \mathcal{I}$, let A_l and A_r be the left and right children of A , respectively. For $A \in \mathcal{I} \cup \mathcal{U} \setminus \{\Omega\}$, let A_p be its parent and A_s be its sibling (i.e., the node in \mathcal{T} that has the same parent as A).

Given \mathcal{T} , it can be shown that the multinomial likelihood of \mathbf{y}_i factorizes into a series of binomial likelihoods at the internal nodes of \mathcal{T} :

$$\mathcal{L}_M(\mathbf{y}_i | \mathbf{p}_i) \propto \prod_{\{A: A \in \mathcal{I}\}} \mathcal{L}_B(y_i(A_l) | y_i(A), \theta_i(A)), \quad (2.3)$$

where

$$y_i(A) = \sum_{\{j: \omega_j \in A\}} y_{ij}, \quad \theta_i(A) = \frac{\sum_{\{j: \omega_j \in A_l\}} p_{ij}}{\sum_{\{j: \omega_j \in A\}} p_{ij}}, \quad (2.4)$$

$$y_i(A_l) | y_i(A), \theta_i(A) \stackrel{\text{ind}}{\sim} \text{Binom}(y_i(A), \theta_i(A)).$$

Note that for $j = 1, \dots, M$, there is a unique path $\mathcal{P}^j = A_0^j = \Omega \rightarrow A_1^j \rightarrow \dots \rightarrow A_{l_j}^j \rightarrow \omega_j$ in \mathcal{T} connecting the root with ω_j such that

$$p_{ij} = \prod_{l=0}^{l_j} \theta_i(A_l^j). \quad (2.5)$$

We denote $\boldsymbol{\theta}_i = \{\theta_i(A) : A \in \mathcal{I}\}$. Let $\boldsymbol{\theta}_i = tr(\mathbf{p}_i)$ and $\mathbf{p}_i = tr^{-1}(\boldsymbol{\theta}_i)$ be the ‘‘tree-based ratio transform’’ and the ‘‘inverse tree-based ratio transform’’ defined in (2.4) and (2.5). \mathbf{p}_i and $\boldsymbol{\theta}_i$ give two equivalent parameterizations of the distribution of \mathbf{y}_i . Figure 2 gives an example of how a specific multinomial parameter $\mathbf{p}_{\text{ex}} = (\frac{5}{12}, \frac{5}{12}, \frac{1}{6}, \frac{1}{6}, \frac{1}{12}, \frac{1}{12})$ on 6 OTUs can be generated sequentially along a given tree.

The factorization in (2.3) provides an orthogonal decomposition of the empirical evidence about \mathbf{p}_i into pieces of ‘‘local’’ evidence about $\theta_i(A)$ at $A \in \mathcal{I}$, which suggests a ‘‘divide-and-conquer’’ strategy of doing inference on \mathbf{p}_i through learning the ‘‘local’’ probability assignment parameters $\boldsymbol{\theta}_i$. To this end, we take the Bayesian strategy and put independent beta priors on the binomial parameters:

$$\theta_i(A) \mid \theta(A), \tau(A) \stackrel{\text{ind}}{\sim} \text{Beta}(\theta(A)\tau(A), (1 - \theta(A))\tau(A)), \quad (2.6)$$

where $\theta(A) \in (0, 1)$ is the prior mean of $\theta_i(A)$, $\tau(A) > 0$ is a dispersion parameter that controls the variability of $\theta_i(A)$ around its mean. Note that the independent priors on $\boldsymbol{\theta}_i$ together with the relation in (2.5) induce a joint prior on \mathbf{p}_i , which falls into the family of Dirichlet-tree distributions (DT) (Dennis III, 1991). Let $\boldsymbol{\theta} = \{\theta(A) : A \in \mathcal{I}\}$ and $\boldsymbol{\tau} = \{\tau(A) : A \in \mathcal{I}\}$, we shall denote the Dirichlet-tree prior on \mathbf{p}_i as

$$\mathbf{p}_i = tr^{-1}(\boldsymbol{\theta}_i), \quad \boldsymbol{\theta}_i \sim \text{DT}_{\boldsymbol{\tau}}(\boldsymbol{\theta}, \boldsymbol{\tau}). \quad (2.7)$$

When $\tau(A) = \tau(A_l) + \tau(A_r)$ for every $A \in \mathcal{I}$ that has non-leaf children, DT degenerates to the Dirichlet distribution. By removing this constraint, DT offers a more flexible way to model the variability of \mathbf{p}_i around its cluster centroid.

DT also induces a more flexible covariance structure than the Dirichlet distribution. This can be seen by considering the covariance between any two categories j_1 and j_2 ($j_1 \neq j_2$). Suppose that the first $(L + 1)$ nodes in \mathcal{P}^{j_1} and \mathcal{P}^{j_2} are shared and let the shared path be $\Omega = A_0 \rightarrow A_1 \rightarrow \dots \rightarrow A_L$. It can be shown that (Dennis III, 1991)

$$\text{Cov}(p_{ij_1}, p_{ij_2}) = \left[\frac{\tau(A_L)}{\tau(A_L) + 1} \prod_{1 \leq t \leq L} \frac{[a(A_t) + 1]\tau(A_{t-1})}{a(A_t)[\tau(A_{t-1}) + 1]} - 1 \right] \mathbb{E}(p_{ij_1})\mathbb{E}(p_{ij_2}), \quad (2.8)$$

where $a(A_t) = \theta(A_{t-1})\tau(A_{t-1})$ if A_t is the left child of A_{t-1} and $a(A_t) = (1 - \theta(A_{t-1}))\tau(A_{t-1})$ otherwise. In DT, the covariance between categories depends not only on their means and the sum of the pseudo count as in the Dirichlet distribution, but also on the tree structure. This offers a more flexible covariance structure among OTU counts governed by the phylogenetic information. For example, since $a(A_t) < \tau(A_{t-1})$, $[a(A_t) + 1]\tau(A_{t-1})/a(A_t)[\tau(A_{t-1}) + 1] > 1$,

p_{ij_1} and p_{ij_2} can be positively correlated if they share a series of common ancestors in the phylogenetic tree. On the other hand, if p_{ij_1} and p_{ij_2} are “far away” in the phylogenetic tree such that their only common ancestor is Ω , $\text{Cov}(p_{ij_1}, p_{ij_2}) = -\mathbb{E}(p_{ij_1})\mathbb{E}(p_{ij_2})/(\tau(\Omega) + 1)$ as in the Dirichlet distribution. When the phylogenetic tree gives decent summaries of the functional relationship among OTUs, this introduces suitable covariance structure among the OTU counts and can improve the inference substantially.

DT has been used for microbiome modelings in various contexts for different purposes. For example, Wang and Zhao (2017) apply the DT multinomial model to study the association between OTU counts and a set of covariates; Tang et al. (2018) and Mao et al. (2020) use the tree decomposition to motivate a divide-and-conquer strategy to increase the statistical power when comparing the OTU composition of groups of samples. In this work, we shall replace the Dirichlet prior in DMM with the DT prior to give a more suitable clustering model for microbiome data. Our first motivation is that when DT is used as the mixing kernel, the model would be more powerful in detecting different clusters. In DMM, if the counts of one OTU are highly variable, the single dispersion parameter would be estimated large in adjustment of this variation. As a result, signals contained in other OTUs would be washed away and the samples would be modeled as drawn from a single cluster. In contrast, the set of dispersion parameters in DT are able to account for different levels of variation across OTUs and thus prevent the signals from being contaminated by the noises.

Specifically, under the multinomial sampling scheme as in DMM, let

$$\begin{aligned} \mathbf{y}_i \mid N_i, \mathbf{p}_i &\stackrel{\text{iid}}{\sim} \text{Multi}(N_i, \mathbf{p}_i) \\ \mathbf{p}_i &= \text{tr}^{-1}(\boldsymbol{\theta}_i) \\ \boldsymbol{\theta}_i \mid \boldsymbol{\pi}, \{(\boldsymbol{\theta}_k^*, \boldsymbol{\tau}_k^*)\}_{k=1}^K &\stackrel{\text{iid}}{\sim} \sum_{k=1}^K \pi_k \text{DT}_{\mathcal{T}}(\boldsymbol{\theta}_k^*, \boldsymbol{\tau}_k^*) \\ \boldsymbol{\pi} = (\pi_1, \dots, \pi_K) &\sim \text{Dir}(\mathbf{b}_0), \end{aligned} \tag{2.9}$$

where

$$(\boldsymbol{\theta}_k^*, \boldsymbol{\tau}_k^*) \stackrel{\text{iid}}{\sim} \text{DT}_{\mathcal{T}}(\boldsymbol{\theta}_0, \boldsymbol{\nu}_0) \times F(\boldsymbol{\tau}), \tag{2.10}$$

$\text{DT}_{\mathcal{T}}(\boldsymbol{\theta}_0, \boldsymbol{\nu}_0)$ the prior for the cluster centroid, $F(\boldsymbol{\tau}) = \prod_{A \in \mathcal{I}} F^A(\tau(A))$ the prior for the within-cluster dispersion. Note that $(\boldsymbol{\theta}_k^*, \boldsymbol{\tau}_k^*)$ determines the k -th “meta-community”. We shall for now refer to this model as the Dirichlet-tree multinomial mixtures (DTMM).

2.3 Discriminative taxa selection

In DMM, all OTUs are treated equally in the clustering procedure. In many applications, however, it is expected that only a (possibly sparse) subset of OTUs determine the underlying clustering. Similarly, under DTMM, not all taxa are necessarily participating in the clustering process. In these cases, it is of scientific interests to identify and report the taxa or OTUs that actually determine the clusters along with the clustering profile. Performing taxa selection in clustering is also of statistical importance. DMM and DTMM introduce

cluster-specific parameters on OTUs or taxa that are not relevant to the latent class, which may overfit the data and can severely limit their statistical power to identify certain clusters. When applied directly in situations where the signal-to-noise ratio is not very large, DMM and DTMM tend to identify a few big clusters containing potential sub-clusters.

In this section, we introduce two modifications to DTMM: firstly, we incorporate a sub-routine in the model to allow automatic taxa selection; secondly, we replace the finite mixture in DTMM with an infinite mixture to avoid presetting the number of clusters, which is equivalent to adopting a Dirichlet process mixture model for the cluster-specific parameters. Formally, for $A \in \mathcal{I}$, let $\gamma(A) \in \{0, 1\}$ be an indicator of whether node A can be contributive to the latent clustering: $\gamma(A) = 1$ if A can play a role in defining clusters, and 0 otherwise. If $\gamma(A) = 1$, A is “active” in clustering and we allow different clusters to have cluster-specific branching probabilities at A ; otherwise, A in “inactive” and we force all the clusters at A to share the same branching probability. For this reason, we shall refer to $\gamma(A)$ and $\lambda(A)$ as the activation indicator and the prior activation probability on A . Let $\boldsymbol{\gamma} = \{\gamma(A) : A \in \mathcal{I}\}$ be the collection of activation indicators of all the internal nodes.

Let $F(\cdot)$ be a probability measure on $(0, \infty)$, $\delta_x(\cdot)$ the Dirac measure. The model can be written in the following hierarchical form:

- sampling model on \mathbf{y}_i :

$$\mathbf{y}_i \mid N_i, \mathbf{p}_i \stackrel{\text{ind}}{\sim} \text{Multi}(N_i, \mathbf{p}_i); \quad (2.11)$$

- priors for the sample-specific probability assignment vector \mathbf{p}_i :

$$\begin{aligned} \mathbf{p}_i &= tr^{-1}(\boldsymbol{\theta}_i) \\ \boldsymbol{\theta}_i \mid \boldsymbol{\theta}'_i, \boldsymbol{\tau}'_i &\stackrel{\text{ind}}{\sim} \text{DT}_{\boldsymbol{\tau}}(\boldsymbol{\theta}'_i, \boldsymbol{\tau}'_i); \end{aligned} \quad (2.12)$$

- priors for the cluster-specific probability assignment vector:

$$\begin{aligned} (\boldsymbol{\theta}'_i, \boldsymbol{\tau}'_i) \mid G &\stackrel{\text{iid}}{\sim} G \\ G &\sim \text{DP}(G_0(\boldsymbol{\theta}, \boldsymbol{\tau} \mid \boldsymbol{\gamma}, \tilde{\boldsymbol{\theta}}, \tilde{\boldsymbol{\tau}}); \beta); \end{aligned} \quad (2.13)$$

- the base measure in DP:

$$\begin{aligned} G_0(\boldsymbol{\theta}, \boldsymbol{\tau} \mid \boldsymbol{\gamma}, \tilde{\boldsymbol{\theta}}, \tilde{\boldsymbol{\tau}}) &= \prod_{A \in \mathcal{I}} G_0^A(\theta(A), \tau(A) \mid \gamma(A), \tilde{\theta}(A), \tilde{\tau}(A)) \\ G_0^A(\theta(A), \tau(A) \mid \gamma(A) = 1, \tilde{\theta}(A), \tilde{\tau}(A)) &= \text{Beta}(\theta_0(A)\nu_0(A), (1 - \theta_0(A))\nu_0(A)) \times F^A(\tau) \\ G_0^A(\theta(A), \tau(A) \mid \gamma(A) = 0, \tilde{\theta}(A), \tilde{\tau}(A)) &= \delta_{(\tilde{\theta}(A), \tilde{\tau}(A))}; \end{aligned} \quad (2.14)$$

- priors for the hyperparameters in the base measure: for $A \in \mathcal{I}$,

$$\begin{aligned} \gamma(A) &\stackrel{\text{ind}}{\sim} \text{Binom}(\lambda(A)) \\ (\tilde{\theta}(A), \tilde{\tau}(A)) &\stackrel{\text{ind}}{\sim} \text{Beta}(\theta_0(A)\nu_0(A), (1 - \theta_0(A))\nu_0(A)) \times F^A(\tau) \\ \lambda(A) &\stackrel{\text{ind}}{\sim} \text{Beta}(a_0(A), b_0(A)). \end{aligned} \quad (2.15)$$

From now on, we shall refer to this model as the Dirichlet-tree multinomial mixtures (DTMM). The graphical model representation of DTMM is shown in [Figure 3](#). Note that G in [\(2.13\)](#) is supported on a countable number of values since samples from a Dirichlet process are discrete, implying ties in the iid samples (θ'_i, τ'_i) 's and thus a clustering on i . This becomes clear with the stick-breaking construction of the Dirichlet process ([Sethuraman, 1994](#)), from which we can rewrite [\(2.12\)](#) and [\(2.13\)](#) as

$$\begin{aligned} \mathbf{p}_i \mid \boldsymbol{\pi}, \{(\boldsymbol{\theta}_k^*, \boldsymbol{\tau}_k^*)\}_{k=1}^\infty &\stackrel{\text{iid}}{\sim} \sum_{k=1}^\infty \pi_k \text{DT}_{\mathcal{T}}(\boldsymbol{\theta}_k^*, \boldsymbol{\tau}_k^*) \\ \pi_k &= v_k \prod_{j=1}^{k-1} (1 - v_j), \text{ where } v_1, v_2, \dots \mid \beta \stackrel{\text{iid}}{\sim} \text{Beta}(1, \beta) \\ (\boldsymbol{\theta}_k^*, \boldsymbol{\tau}_k^*) &\stackrel{\text{iid}}{\sim} G_0(\boldsymbol{\theta}, \boldsymbol{\tau} \mid \boldsymbol{\gamma}, \tilde{\boldsymbol{\theta}}, \tilde{\boldsymbol{\tau}}). \end{aligned} \tag{2.16}$$

For $i = 1, \dots, n$, let $c_i \in \mathbb{N}^+$ be the cluster label for the i -th sample such that $\mathbf{p}_i \mid c_i, \{(\boldsymbol{\theta}_k^*, \boldsymbol{\tau}_k^*)\}_{k=1}^\infty \sim \text{DT}_{\mathcal{T}}(\boldsymbol{\theta}_{c_i}^*, \boldsymbol{\tau}_{c_i}^*)$. We can equivalently illustrate DTMM as in [Figure 4](#). For comparison, we can introduce the latent cluster labels to DMM and DTMM without taxa selection in the same manner and write their graphical model representations as in [Figure 5](#) and [Figure 6](#). [Figure 6](#) and [Figure 4](#) illustrate how DTMM is generalized in this section.

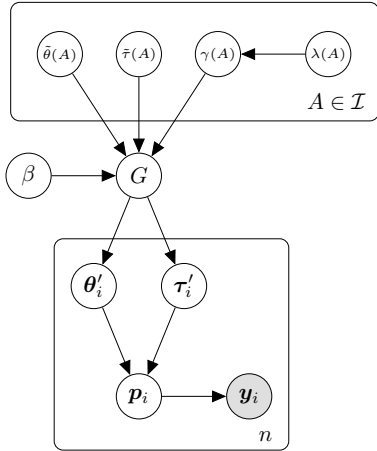


Figure 3: A graphical model representation of DTMM.

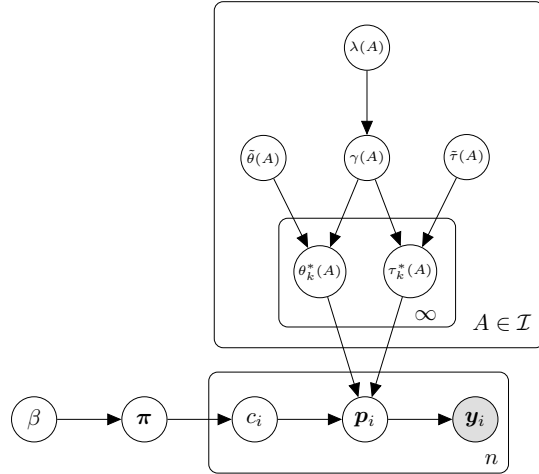


Figure 4: An alternative graphical model representation of DTMM.

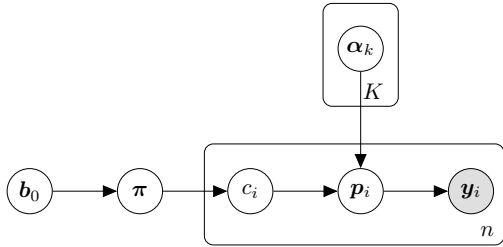


Figure 5: A graphical model representation of DMM.

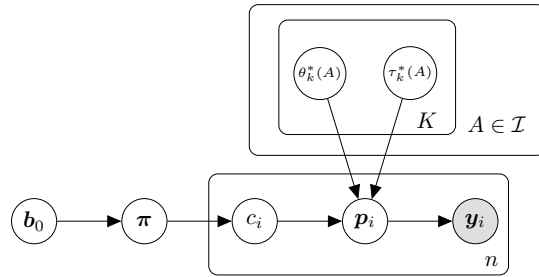


Figure 6: A graphical model representation of DTMM without taxa selection.

Prior specification. To complete the model specification, we need to choose $a_0(A)$, $b_0(A)$, $\theta_0(A)$, $\nu_0(A)$ and $F^A(\tau)$ for each $A \in \mathcal{I}$. Ideally, informative prior knowledge shall be incorporated in choosing these parameters. If instead no prior knowledge is available, we treat these parameters (priors) as global such that they do not dependent on A and remove the “ (A) ’s” from the notations.

For the coupling probability λ , we could set $a_0 = b_0 = 1$ such that λ has a uniform distribution *a priori*, which yields the following prior probability on the $\gamma(A)$ ’s (Scott and Berger, 2010):

$$\Pr(\boldsymbol{\gamma}) = \frac{1}{M} \left(\sum_{A \in \mathcal{I}} \gamma(A) \right)^{-1}. \quad (2.17)$$

This prior allows multiplicity adjustment in the taxa selection. A default choice for (θ_0, ν_0) is $(0.5, 1)$, which yields the Jeffrey’s prior on $\theta_k^*(A)$ and $\theta^*(A)$. For $F(\gamma)$, any prior with a reasonably large support that covers a wide range of dispersion levels can be chosen. For example, we let $F(\tau)$ have density $f(\tau) = (\tau \times 5 \log 10)^{-1} \mathbb{1}_{(0.1 \leq \tau \leq 10^4)}$, which is equivalent to putting the $\text{Unif}(-1, 4)$ prior on $\log_{10} \tau$. Figure 7 shows the histogram of 10^6 draws of τ from this $F(\tau)$. In our software, we use a discrete approximation of this prior induced by drawing $\log_{10} \tau$ uniformly from $\{-1, -0.5, 0, 0.5, 1, \dots, 4\}$.

Model behavior. In our formulation, $\boldsymbol{\theta}$ and $\boldsymbol{\tau}$ with a superscript “*” are cluster-specific parameters that govern the centroid and the within cluster variance of each cluster. $\boldsymbol{\theta}$ and $\boldsymbol{\tau}$ with a “~” are parameters that determine the centroid and the variability of the “coupled” base distribution. For $i = 1, \dots, n$, recall that $c_i \in \mathbb{N}^+$ is the cluster label for the i -th sample. Moreover, let $\mathbf{c} = (c_1, c_2, \dots, c_n)$, \mathbf{c}^* the set of distinct values in \mathbf{c} and $k^* = |\mathbf{c}^*|$ the number of distinct clusters. We note that the actual values of c_i bear no significance and thus assume that the c_i ’s take integer values between 1 and $|\mathbf{c}^*|$. At each node $A \in \mathcal{I}$, $\gamma(A)$ serves as a selector: $\tilde{\theta}(A)$ and $\tilde{\tau}(A)$ become relevant only if $\gamma(A) = 0$. If $\gamma(A) = 1$, they are masked and not used by the model. We note that this “masking” happens at the level of the base distribution of the Dirichlet process mixture model. If $\gamma(A) = 0$, the base distribution G_0^A is a point mass. Thus $(\theta'_i(A), \tau'_i(A))$ ’s must share the same value although $(\boldsymbol{\theta}'_i, \boldsymbol{\tau}'_i)$ ’s may not be the same. In a special case when $\gamma(A) = 0$ for all $A \in \mathcal{I}$, the entire base distribution is a point mass and $(\boldsymbol{\theta}'_i, \boldsymbol{\tau}'_i)$ ’s are all the same. In this case, the cluster

labels \mathbf{c} are only nominal—the samples are from a single cluster although it is possible that $|\mathbf{c}^*| > 1$. Similarly, $\gamma(A)$ as an OTU selector is also nominal— A is not necessarily relevant to clustering even if $\gamma(A) = 1$. In real applications, what we care are not these “nominal” parameters \mathbf{c} and γ *per se*, but their “actual” counterparts. Specifically, let $g_i \in \mathbb{N}^+$ be the “actual” cluster label of sample i for $i = 1, \dots, n$, and let $s(A) \in \{0, 1\}$ be the “actual” indicator of whether A is relevant to clustering for $A \in \mathcal{I}$. Moreover, let $\mathbf{g} = (g_1, \dots, g_n)$ and $\mathbf{s} = \{s(A) : A \in \mathcal{I}\}$. We have

$$\mathbf{g} = \begin{cases} \mathbf{c}, & \text{if } \gamma \neq \mathbf{0}_{M-1} \text{ and } \mathbf{c} \neq \mathbf{1}_n \\ \mathbf{1}_n, & \text{if } \gamma = \mathbf{0}_{M-1} \text{ or } \mathbf{c} = \mathbf{1}_n, \end{cases} \quad (2.18)$$

and

$$\mathbf{s} = \begin{cases} \gamma, & \text{if } \mathbf{c} \neq \mathbf{1}_n, \text{ and } \gamma \neq \mathbf{0}_{M-1} \\ \mathbf{0}_{M-1}, & \text{if } \mathbf{c} = \mathbf{1}_n \text{ or } \gamma = \mathbf{0}_{M-1}. \end{cases} \quad (2.19)$$

Unlike \mathbf{c} and γ , \mathbf{g} and \mathbf{s} are directly interpretable. For example, $A \in \mathcal{I}$ is relevant to clustering if and only if $s(A) = 1$. In microbiome applications, it is typically expected that the samples have a latent clustering pattern. Therefore, it is common that $\mathbf{g} = \mathbf{c}$ and $\mathbf{s} = \gamma$.

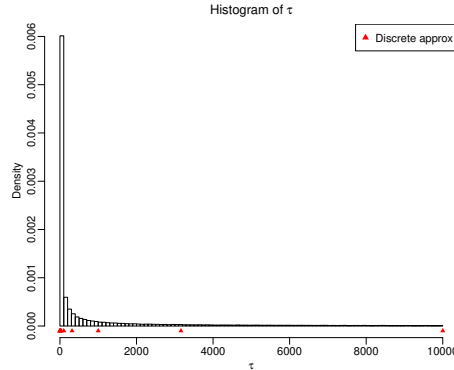


Figure 7: Histogram of τ . The discrete prior puts equal mass at the red points.

2.4 Inference strategy

Under DTMM, we are interested in inferring the nominal cluster labels \mathbf{c} and the nominal coupling indicator γ from which the actual cluster labels \mathbf{g} and the actual coupling indicators \mathbf{s} can be obtained. Let \mathbf{y}_{-i} denote all the observations other than \mathbf{y}_i . Bayesian inference for DTMM can be achieved by constructing a Markov chain that converges to the joint posterior of (\mathbf{c}, γ) . We shall see that techniques designed for Dirichlet process mixture models in general, such as those described in Neal (2000) or Ishwaran and James (2001), can be applied here.

For $c \in \mathbf{c}^*$, let $\psi_c^* = (\theta_c^*, \tau_c^*)$ be the parameters that define the cluster indicated by c (we also let $\psi_c^*(A) = (\theta_c^*(A), \tau_c^*(A))$ for $A \in \mathcal{I}$). Similarly, let $\tilde{\psi} = (\tilde{\theta}, \tilde{\tau})$ be the shared

parameters at the coupled nodes and $\tilde{\boldsymbol{\psi}}(A) = (\tilde{\theta}(A), \tilde{\tau}(A))$ for $A \in \mathcal{I}$. The set of unknown parameters in DTMM is $\{\{\boldsymbol{\theta}_i, c_i\}_{i=1}^n, \{\boldsymbol{\psi}_c^*\}_{c=1}^{k^*}, \boldsymbol{\gamma}, \tilde{\boldsymbol{\psi}}, \beta, \lambda\}$. In this work, we construct a collapsed Gibbs sampler that iteratively samples from the joint posterior of $(\mathbf{c}, \boldsymbol{\gamma}, \beta, \lambda)$. The key to our inference strategy is to compute the marginal likelihoods of samples from a given cluster, integrating out both the sample-specific parameter $\boldsymbol{\theta}_i$ and the cluster-specific parameter $\boldsymbol{\psi}_c^*$. This can be achieved numerically due to two facts. Firstly, the beta-binomial conjugacy makes it easy to integrate out the sample-specific compositional probabilities $\boldsymbol{\theta}_i$. Secondly, the tree-based decomposition of the Dirichlet distribution and the multinomial likelihood provides a divide-and-conquer strategy to marginalize out the high-dimensional cluster-specific parameters $\boldsymbol{\psi}_c^*$ through performing a series of low-dimensional integrals at the internal nodes of the tree.

Specifically, for any $c \in \mathbf{c}^*$, let $\mathbf{Y}_c^I = \{\mathbf{y}_i : c_i = c, i \in I\}$ be a set of samples in cluster c where $I \subset [n] := \{1, \dots, n\}$. We also let $\mathbf{Y}_c = \mathbf{Y}_c^{[n]}$ be the set of all samples in cluster c and $\mathbf{Y}_c^{-i} = \mathbf{Y}_c^{[n] \setminus \{i\}}$ be the set of samples in cluster c excluding sample i . For $A \in \mathcal{I}$, let $\mathcal{L}^A(\mathbf{Y}_c^I | \boldsymbol{\psi}_c^*(A), \boldsymbol{\gamma}(A), \tilde{\boldsymbol{\psi}}(A))$ be the marginal likelihood of \mathbf{Y}_c^I at node A by marginalizing out the sample-specific parameters. The beta-binomial conjugacy yields

$$\begin{aligned} & \mathcal{L}^A(\mathbf{Y}_c^I | \boldsymbol{\psi}_c^*(A), \boldsymbol{\gamma}(A), \tilde{\boldsymbol{\psi}}(A)) \\ &= \prod_{\{i \in I: c_i = c\}} \binom{y_i(A)}{y_i(A_l)} \frac{B(\boldsymbol{\theta}_c^*(A)\boldsymbol{\tau}_c^*(A) + y_i(A_l), (1 - \boldsymbol{\theta}_c^*(A))\boldsymbol{\tau}_c^*(A) + y_i(A_r))}{B(\boldsymbol{\theta}_c^*(A)\boldsymbol{\tau}_c^*(A), (1 - \boldsymbol{\theta}_c^*(A))\boldsymbol{\tau}_c^*(A))}. \end{aligned} \quad (2.20)$$

We then further integrate out $\boldsymbol{\psi}_c^*(A)$ to obtain the marginal likelihood of \mathbf{Y}_c^I at node A given only the coupling indicators and the base parameters:

$$\begin{aligned} \mathcal{L}_1^A(\mathbf{Y}_c^I) &:= \iint \mathcal{L}^A(\mathbf{Y}_c^I | \boldsymbol{\psi}_c^*(A), \boldsymbol{\gamma}(A) = 1, \tilde{\boldsymbol{\psi}}(A)) d\Pi(\boldsymbol{\psi}_c^*(A) | \boldsymbol{\gamma}(A) = 1, \tilde{\boldsymbol{\psi}}(A)) \\ &= \iint \prod_{\{i \in I: c_i = c\}} \binom{y_i(A)}{y_i(A_l)} \frac{B(\boldsymbol{\theta}(A)\boldsymbol{\tau}(A) + y_i(A_l), (1 - \boldsymbol{\theta}(A))\boldsymbol{\tau}(A) + y_i(A_r))}{B(\boldsymbol{\theta}(A)\boldsymbol{\tau}(A), (1 - \boldsymbol{\theta}(A))\boldsymbol{\tau}(A))} \\ &\quad \times \frac{\boldsymbol{\theta}(A)^{\boldsymbol{\theta}_0(A)\boldsymbol{\nu}_0(A)-1} (1 - \boldsymbol{\theta}(A))^{(1-\boldsymbol{\theta}_0(A))\boldsymbol{\nu}_0(A)-1}}{B(\boldsymbol{\theta}_0(A)\boldsymbol{\nu}_0(A), (1 - \boldsymbol{\theta}_0(A))\boldsymbol{\nu}_0(A))} d\boldsymbol{\theta}(A) dF^A(\boldsymbol{\tau}), \end{aligned} \quad (2.21)$$

$$\begin{aligned} \mathcal{L}_0^A(\mathbf{Y}_c^I | \tilde{\boldsymbol{\psi}}(A)) &:= \iint \mathcal{L}^A(\mathbf{Y}_c^I | \boldsymbol{\psi}_c^*(A), \boldsymbol{\gamma}(A) = 0, \tilde{\boldsymbol{\psi}}(A)) d\Pi(\boldsymbol{\psi}_c^*(A) | \boldsymbol{\gamma}(A) = 0, \tilde{\boldsymbol{\psi}}(A)) \\ &= \prod_{\{i \in I: c_i = c\}} \binom{y_i(A)}{y_i(A_l)} \frac{B(\tilde{\boldsymbol{\theta}}(A)\tilde{\boldsymbol{\tau}}(A) + y_i(A_l), (1 - \tilde{\boldsymbol{\theta}}(A))\tilde{\boldsymbol{\tau}}(A) + y_i(A_r))}{B(\tilde{\boldsymbol{\theta}}(A)\tilde{\boldsymbol{\tau}}(A), (1 - \tilde{\boldsymbol{\theta}}(A))\tilde{\boldsymbol{\tau}}(A))}. \end{aligned} \quad (2.22)$$

Note that the integrals in (S1) are two-dimensional integrals that are easy to evaluate numerically. In comparison, to perform a fully Bayesian inference for DMM, the high dimensional cluster centroids $\boldsymbol{\alpha}_k$'s in (2.2) has to either be integrated out directly or incorporated into the MCMC procedure. With these marginal likelihoods, we can summarize the full conditionals of the parameters as follows. Details on the derivation of these full conditionals are given in the online supplementary materials A.

The full conditional of γ : For each $A \in \mathcal{I}$, the Bayes factor comparing $\gamma(A) = 1$ versus $\gamma(A) = 0$ given \mathbf{c} can be written as

$$M_{10}(A \mid \gamma^{-A}, \mathbf{c}, \beta, \lambda) = M_{10}(A \mid \mathbf{c}) = \frac{\prod_{c \in \mathbf{c}^*} \mathcal{L}_1^A(\mathbf{Y}_c)}{\int \mathcal{L}_0^A(\mathbf{Y} \mid \tilde{\psi}(A)) d\Pi(\tilde{\psi}(A))}. \quad (2.23)$$

It follows that

$$\Pr(\gamma(A) = 1 \mid \mathbf{Y}, \gamma^{-A}, \mathbf{c}, \beta, \lambda) = \frac{\lambda M_{10}(A \mid \mathbf{c})}{(1 - \lambda) + \lambda M_{10}(A \mid \mathbf{c})}. \quad (2.24)$$

The full conditional of \mathbf{c} : For $i = 1, \dots, n$, let $\mathbf{c}_{-i} = \mathbf{c} \setminus \{c_i\}$. Following the discussion in [Neal \(2000\)](#), we can write the prior conditional distribution of c_i given \mathbf{c}_{-i} as

$$\begin{aligned} \Pr(c_i = c \text{ for some } c \in \mathbf{c}_{-i} \mid \mathbf{c}_{-i}, \gamma, \beta, \lambda) &= \frac{n_{-i,c}}{n - 1 + \beta} \\ \Pr(c_i \neq c_j \text{ for all } j \neq i \mid \mathbf{c}_{-i}, \gamma, \beta, \lambda) &= \frac{\beta}{n - 1 + \beta}, \end{aligned} \quad (2.25)$$

where $n_{-i,c}$ represents the number of samples in the cluster with label c excluding sample i . After conditioning on the data, these probabilities become

$$\begin{aligned} \Pr(c_i = c \text{ for some } c \in \mathbf{c}_{-i} \mid \mathbf{c}_{-i}, \mathbf{Y}, \gamma, \beta, \lambda) &\propto n_{-i,c} \times \frac{\mathcal{L}_1(\mathbf{y}_i, \mathbf{Y}_c^{-i} \mid \gamma)}{\mathcal{L}_1(\mathbf{Y}_c^{-i} \mid \gamma)} \\ \Pr(c_i \neq c_j \text{ for all } j \neq i \mid \mathbf{c}_{-i}, \mathbf{Y}, \gamma, \beta, \lambda) &\propto \beta \times \mathcal{L}_1(\mathbf{y}_i \mid \gamma), \end{aligned} \quad (2.26)$$

where for any $\mathbf{y}_i, \dots, \mathbf{y}_l$ in the same cluster,

$$\mathcal{L}_1(\mathbf{y}_1, \dots, \mathbf{y}_l \mid \gamma) = \prod_{\{A \in \mathcal{I}: \gamma(A)=1\}} \mathcal{L}_1^A(\mathbf{y}_1, \dots, \mathbf{y}_l). \quad (2.27)$$

If $\gamma(A) = 0$ for every $A \in \mathcal{I}$, we let $\mathcal{L}_1(\mathbf{y}_1, \dots, \mathbf{y}_l) = 1$. Note that given the coupling status γ , the posterior conditional distribution of c_i only depends on the likelihoods of the data at nodes with $\gamma(A) = 1$. Therefore, to update the cluster label for any observation \mathbf{y}_i , we only need to focus on the nodes with $\gamma(A) = 1$ and at each of these nodes compute: (i) the marginal likelihood of \mathbf{y}_i and (ii) for each $c \in \mathbf{c}_{-i}$, the conditional likelihood of \mathbf{y}_i given \mathbf{Y}_c^{-i} . All nodes with $\gamma(A) = 0$ and thus the parameters at these nodes are essentially ‘‘nuisance’’ for the cluster labels.

The full conditional of β : Instead of fixing β , one can put a prior on it and incorporate it into the Gibbs sampler. For example, when gamma priors are used, [Escobar and West \(1995\)](#) update β using a data augmentation trick. When arbitrary priors are used, β can be

updated by reparameterizing $b = \frac{\beta}{\beta+1}$ (Hoff et al., 2006). Specifically, let $\pi(b)$ be the induced prior on b , we have

$$\pi(b \mid \mathbf{Y}, \mathbf{c}, \boldsymbol{\gamma}, \lambda) \propto \pi(b) \times \left(\frac{b}{1-b} \right)^{|\mathbf{c}^*|} \frac{\Gamma(b/(1-b))}{\Gamma(b/(1-b) + n)}. \quad (2.28)$$

The full conditional of λ : By the beta-binomial conjugacy,

$$\lambda \mid \mathbf{Y}, \mathbf{c}, \boldsymbol{\gamma}, \beta \sim \text{Beta} \left(a_0 + \sum_{A \in \mathcal{I}} \gamma(A), b_0 + \sum_{A \in \mathcal{I}} (1 - \gamma(A)) \right). \quad (2.29)$$

Details for implementing the Gibbs sampler are summarized in Algorithm 1. After running the chain for T iterations, we discard the first B samples as burn-in and obtain $(T - B)$ posterior samples denoted as $[\{\mathbf{c}^{(B+1)}, \boldsymbol{\gamma}^{(B+1)}, \beta^{(B+1)}, \lambda^{(B+1)}\}, \dots, \{\mathbf{c}^{(T)}, \boldsymbol{\gamma}^{(T)}, \beta^{(T)}, \lambda^{(T)}\}]$. Based on these posterior samples, we can compute the posterior samples for \mathbf{g} and \mathbf{s} based on (2.18) and (2.19). We denote these posterior samples as $[\{\mathbf{g}^{(B+1)}, \mathbf{s}^{(B+1)}\}, \dots, \{\mathbf{g}^{(T)}, \mathbf{s}^{(T)}\}]$

For each sample $\mathbf{g}^{(t)}$, let $\Gamma^{(t)}$ be the corresponding $n \times n$ association matrix whose (i_1, i_2) element is 1 if $g_{i_1}^{(t)} = g_{i_2}^{(t)}$ and 0 otherwise. Element-wise average of $\Gamma^{(B+1)}, \dots, \Gamma^{(T)}$ provides an estimation $\hat{\Pi}$ of the pairwise clustering probability matrix Π whose (i_1, i_2) element is $\Pr(\mathbf{y}_{i_1}$ and \mathbf{y}_{i_2} in the same cluster). To yield a representative clustering, we can report the least-squares model-based clustering (Dahl, 2006), defined as

$$\mathbf{C}_{LS} = \arg \min_{\{\mathbf{g}^{(t)}: B < t \leq T\}} \sum_{1 \leq i_1 \leq n} \sum_{1 \leq i_2 \leq n} (\Gamma_{i_1 i_2}^{(t)} - \hat{\Pi}_{i_1 i_2})^2. \quad (2.30)$$

\mathbf{C}_{LS} has the advantage that it incorporates information from all posterior samples while output one of the observed clustering in the Markov Chain (Dahl, 2006). Other representative clusterings such as the MAP clustering or the clustering given by the last iteration are also frequently used.

We can also portray the cluster centroids given any representative clustering and the corresponding coupling indicators. Suppose that $\mathbf{c}_{rep} = \mathbf{g}^{(t_0)}$ for $B < t_0 \leq T$ is one of the representative clusterings and let $\boldsymbol{\gamma}_{rep} = \mathbf{s}^{(t_0)}$. For the k -th resulting cluster defined by \mathbf{c}_{rep} , $1 \leq k \leq |\mathbf{c}_{rep}^*|$, the posterior mean of the branching probability at $A \in \mathcal{I}$ given the coupling status $\gamma_{rep}(A)$ can be written as

$$\begin{aligned} \mathbb{E}[\theta_k^*(A) \mid \mathbf{Y}, \gamma_{rep}(A) = 1] &= \iint \theta_k^*(A) \times \pi(\theta_k^*(A), \tau_k^*(A) \mid \mathbf{Y}_k) d\theta_k^*(A) d\tau_k^*(A) \\ \mathbb{E}[\tilde{\theta}(A) \mid \mathbf{Y}, \gamma_{rep}(A) = 0] &= \iint \tilde{\theta}(A) \times \pi(\tilde{\theta}(A), \tilde{\tau}(A) \mid \mathbf{Y}) d\tilde{\theta}(A) d\tilde{\tau}(A) \end{aligned} \quad (2.31)$$

Algorithm 1 Gibbs sampler for DTMM

procedure GIBBS($B, T, \{\mathbf{y}_1, \dots, \mathbf{y}_n\}$) $\triangleright B$: burn-in; T : total number of iterations.

Initialize $\mathbf{c}^{(0)}, \boldsymbol{\gamma}^{(0)}, \beta^{(0)}, \gamma^{(0)}$.

for $t = 1, 2, \dots, T$ **do**

[2] **Update the coupling indicators:**

for $A \in \mathcal{I}$ **do**

Compute $M_{10}^{(t-1)}(A | \mathbf{c}^{(t-1)})$ as defined by (2.24).

Draw a new value for $\gamma^{(t)}(A) \sim \text{Binom} \left(1, \frac{\lambda^{(t-1)} M_{10}^{(t-1)}(A | \mathbf{c}^{(t-1)})}{(1-\lambda^{(t-1)}) + \lambda^{(t-1)} M_{10}^{(t-1)}(A | \mathbf{c}^{(t-1)})} \right)$.

end for

[1] **Update the cluster labels:**

for $i = 1, 2, \dots, n$ **do**

Draw a new value for $c_i^{(t)}$ from

$$c_i | c_1^{(t)}, \dots, c_{i-1}^{(t)}, c_{i+1}^{(t-1)}, \dots, c_n^{(t-1)}, \mathbf{Y}, \boldsymbol{\gamma}^{(t)}, \beta^{(t-1)}$$

as defined by (2.26).

end for

[3] **Update the Dirichlet process precision parameter:**

Draw value b^{new} from $b \sim \pi(b | \mathbf{Y}, \mathbf{c}^{(t)}, \boldsymbol{\gamma}^{(t)}, \lambda^{(t-1)})$ as defined in (2.28).

Let $\beta^{(t)} = \frac{b^{\text{new}}}{1-b^{\text{new}}}$.

[4] **Update the prior coupling probabilities:**

Draw $\lambda^{(t)}$ from $\lambda | \mathbf{Y}, \mathbf{c}^{(t)}, \boldsymbol{\gamma}^{(t)}, \beta^{(t)}$ as defined in (2.29).

end for

return $[\{\mathbf{c}^{(B+1)}, \boldsymbol{\gamma}^{(B+1)}, \beta^{(B+1)}, \lambda^{(B+1)}\}, \dots, \{\mathbf{c}^{(T)}, \boldsymbol{\gamma}^{(T)}, \beta^{(T)}, \lambda^{(T)}\}]$.

end procedure

where

$$\begin{aligned} \pi(\theta_k^*(A), \tau_k^*(A) | \mathbf{Y}_k) &\propto \prod_{\mathbf{y}_i \in \mathbf{Y}_K} \binom{y_i(A)}{y_i(A_i)} \frac{B(\theta_k^*(A)\tau_k^*(A) + y_i(A_i), (1 - \theta_k^*(A))\tau_k^*(A) + y_i(A_r))}{B(\theta_k^*(A)\tau_k^*(A), (1 - \theta_k^*(A))\tau_k^*(A))} \\ &\quad \times \pi(\theta_k^*(A), \tau_k^*(A)) \\ \pi(\tilde{\theta}(A), \tilde{\tau}(A) | \mathbf{Y}) &\propto \mathcal{L}_0^A(\mathbf{Y} | \tilde{\boldsymbol{\psi}}(A)) \times \pi(\tilde{\theta}(A), \tilde{\tau}(A)). \end{aligned} \tag{2.32}$$

Note that (2.31) involves two-dimensional integrals that can be numerically approximated accurately. Let $\bar{\mathbf{p}}_k = (\bar{p}_{k1}, \dots, \bar{p}_{kM})$ be the posterior mean of \mathbf{p}_k^* , which is the centroid of the k -th cluster. For $\omega_j \in \Omega$, let $A_0^j \rightarrow A_1^j \rightarrow \dots \rightarrow A_j^j \rightarrow \omega_j$ be the unique path in \mathcal{T}

connecting Ω and ω_j . Then

$$\begin{aligned} \bar{p}_{kj} &= \prod_{l=0}^{l_j} \mathbb{E}[\theta_k^*(A_l^j) \mid \mathbf{Y}, \gamma_{rep}(A_l^j) = 1]^{\mathbb{1}(\gamma_{rep}(A_l^j)=1)} \\ &\quad \times \mathbb{E}[\tilde{\theta}(A_l^j) \mid \mathbf{Y}, \gamma_{rep}(A_l^j) = 0]^{\mathbb{1}(\gamma_{rep}(A_l^j)=0)}. \end{aligned} \quad (2.33)$$

Note that \bar{p}_k only characterizes the centroid of the k -th cluster. To characterize the within-cluster dispersion, we need to look at the posterior distribution of $\tau_k^*(A)$ or $\tilde{\tau}(A)$ for $A \in \mathcal{I}$, which is available through marginalizing out $\theta_k^*(A)$ or $\tilde{\theta}(A)$ in (2.32).

2.5 Sample classification for microbiome data with DTMM

The DTMM framework can also be used in the supervised setting to achieve sample classification based on a training microbiome dataset. Without loss of generality, suppose that the training dataset contains microbiome samples from K classes: $\{(\mathbf{y}_1, c_1), (\mathbf{y}_2, c_2), \dots, (\mathbf{y}_n, c_n)\}$, $1 \leq c_i \leq K$. We consider the following generative model of \mathbf{Y} :

$$\begin{aligned} \mathbf{y}_i \mid c_i = k &\stackrel{\text{ind}}{\sim} \text{DT}_{\mathcal{T}}(\boldsymbol{\theta}_k^*, \boldsymbol{\tau}_k^*) \\ (\boldsymbol{\theta}_k^*, \boldsymbol{\tau}_k^*) &\stackrel{\text{iid}}{\sim} G_0(\boldsymbol{\theta}, \boldsymbol{\tau} \mid \boldsymbol{\gamma}, \tilde{\boldsymbol{\theta}}, \tilde{\boldsymbol{\tau}}) \\ \Pr(c_i = k) &= \pi_k, \end{aligned} \quad (2.34)$$

where G_0 and the hyperparameters of G_0 are specified as in (2.14) and (2.15).

Let \mathbf{y}^{new} be a new microbiome sample from (2.34). It follows that

$$\begin{aligned} \Pr(c^{new} = k \mid \mathbf{y}^{new}, \mathbf{Y}) &\propto \pi_k \mathcal{L}(\mathbf{y}^{new} \mid c^{new} = k, \mathbf{Y}) \\ &\propto \sum_{\boldsymbol{\gamma}} \pi(\boldsymbol{\gamma} \mid \mathbf{Y}) \iint \mathcal{L}(\mathbf{y}^{new} \mid \boldsymbol{\psi}_k^*, \boldsymbol{\gamma}, \tilde{\boldsymbol{\psi}}, \mathbf{Y}_k) d\Pi(\boldsymbol{\psi}_k^* \mid \mathbf{Y}_k, \boldsymbol{\gamma}, \tilde{\boldsymbol{\psi}}) d\Pi(\tilde{\boldsymbol{\psi}} \mid \mathbf{Y}). \end{aligned} \quad (2.35)$$

Note that (2.35) can be numerically evaluated in a way similar to the marginal likelihood evaluation in DTMM. Details of doing inference for classification under the DTMM framework can be found in the online supplementary materials A.3.

3 Numerical examples

3.1 Simulation studies

In this section, we carry out a series of simulation studies to evaluate the performance of DTMM and compare it to several other methods for clustering microbiome count data—namely, the Dirichlet multinomial mixtures (DMM) (Holmes et al., 2012), the k -means algorithm (K-ms) (Lloyd, 1982), the partitioning around medoids algorithm (PAM) (Kaufman and Rousseeuw, 2009), hierarchical clustering (Hclust) (Kaufman and Rousseeuw, 2009), and spectral clustering (Spec) (Ng et al., 2002).

3.1.1 Simulation setup

In the numerical examples, we simulate datasets with n samples and six OTUs. In each dataset, the n samples are denoted as $\mathbf{y}_i = (y_{i1}, \dots, y_{i6})$, $i = 1, \dots, n$, which are generated from the following model:

$$\begin{aligned} \mathbf{y}_i | N_i, \mathbf{p}_i &\stackrel{\text{iid}}{\sim} \text{Multi}(N_i, \mathbf{p}_i) \\ \mathbf{p}_i &\stackrel{\text{iid}}{\sim} \sum_{k=1}^K \pi_k \cdot H_k(\mathbf{p}_i | \boldsymbol{\beta}_k) \\ N_i &\stackrel{\text{iid}}{\sim} \text{Neg-Binom}(m, s), \end{aligned} \quad (3.1)$$

where the mixture kernel $H_k(\mathbf{p}_i | \boldsymbol{\beta}_k)$ is a distribution on the 5-simplex with parameter $\boldsymbol{\beta}_k$. We take the tree in [Figure 8](#) as the “phylogenetic tree” over the six OTUs and use it as the \mathcal{T} when fitting DTMM. We consider 5 different simulation scenarios by choosing different mixture kernels $H_k(\mathbf{p}_i | \boldsymbol{\beta}_k)$ in (3.1). In each scenario, we let $n = 90$ or 180 , $K = 3$ and $(\pi_1, \pi_2, \pi_3) = (\frac{4}{9}, \frac{3}{9}, \frac{2}{9})$. Parameters for the negative-binomial distribution are chosen as $m = 15000$, $s = 20$ such that the generated total counts has mean 15000 and standard deviation 3346, with 95% of them fall into the range (9158, 22258). In the 5 simulation scenarios, the mixture kernels are chosen as follows:

- I. **Dirichlet-tree kernel.** We first fix $\mathcal{T} = \mathcal{T}_6$ as in [Figure 8](#) and let $H_k(\mathbf{p}_i | \boldsymbol{\beta}_k) = \text{DT}_{\mathcal{T}}(\boldsymbol{\theta}_k, \boldsymbol{\tau}_k)$ such that DTMM is the “true” model. The parameters $(\boldsymbol{\theta}_k, \boldsymbol{\tau}_k)$ are chosen such that the branching probabilities at the 5 internal nodes have the Beta distributions as shown in [Figure 9](#), where $\boldsymbol{\nu}_1 = (10\alpha, 2\alpha)$, $\boldsymbol{\nu}_2 = (6\alpha, 6\alpha)$, $\boldsymbol{\nu}_3 = (2\alpha, 10\alpha)$ and $\gamma = 0.1$. We write this specific family of Dirichlet-tree distributions as $\text{DT}_{\mathcal{T}_6}(\boldsymbol{\nu}_k; \alpha; \tau)$, $k = 1, 2, 3$. Note that when $\alpha = \gamma$, the Dirichlet-tree distribution becomes the Dirichlet distribution. In this case, only the branching probabilities at node C contribute to the clustering. The signals are thus local to a single node. Three signal levels are considered by letting $\alpha = 1, 3, 6$.

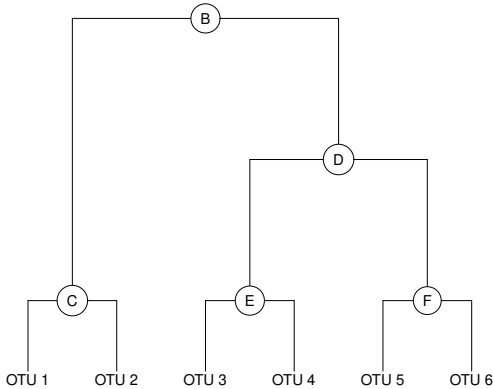


Figure 8: The phylogenetic tree for the simulated examples.

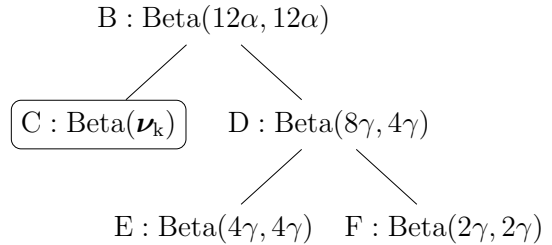


Figure 9: Distributions for the branching probabilities in Scenario I.

II. **Dirichlet kernel.** In this scenario, we let $H_k(\mathbf{p}_i | \boldsymbol{\beta}_k) = \text{Dir}(\boldsymbol{\alpha}_k)$ such that DMM is the “true” model that generates the data. In this case, DTMM is still correct but is over-specified. We let $\boldsymbol{\alpha}_1 = (2, 2, 5, 2, 3, 1) \cdot \alpha_0$, $\boldsymbol{\alpha}_2 = (2, 4, 3, 2, 1, 3) \cdot \alpha_0$ and $\boldsymbol{\alpha}_3 = (2, 6, 1, 2, 2, 2) \cdot \alpha_0$ for $\alpha_0 > 0$ such that all six OTUs are active in differentiating the clusters and the signals are global. We consider three signal levels with $\alpha_0 = 1, 3, 5$.

In the following three examples, we evaluate the performance of DTMM when the model is misspecified. Let $\mathbf{p} = (p_1, \dots, p_6) \in \mathbb{S}^5$. We say that \mathbf{p} has the logistic normal distribution (Atchison and Shen, 1980) and denote as $\mathbf{p} \sim \text{Logit-Norm}(\boldsymbol{\mu}, \boldsymbol{\Sigma})$ if

$$\mathbf{x} = \left(\log \left(\frac{p_1}{p_6} \right), \dots, \log \left(\frac{p_5}{p_6} \right) \right)^\top$$

$$\mathbf{x} \stackrel{\text{ind}}{\sim} \text{N}(\boldsymbol{\mu}, \boldsymbol{\Sigma}).$$

In Scenarios III, IV and V, we let $H_k(\mathbf{p}_i | \boldsymbol{\beta}_k) = \text{Logit-Norm}(\boldsymbol{\mu}_k, \boldsymbol{\Sigma}_k)$. In these examples, we assume that the phylogenetic tree \mathcal{T}_6 provides some insights on the covariate structures of the OTUs.

III. **Logistic-normal approximations to the Dirichlet-tree kernel.** Consider the Dirichlet-tree kernels $q_k = \text{DT}_{\mathcal{T}_6}(\boldsymbol{\nu}_k; \alpha; \tau)$ as in Scenario I with $\gamma = 0.5$ for $k = 1, 2, 3$. In this example, we let

$$H_k(\mathbf{p}_i | \boldsymbol{\beta}_k) = \arg \min_{h \in \mathbb{L}^5} D_{\text{KL}}(q_k \| h)$$

where $D_{\text{KL}}(q_k \| h)$ is the Kullback-Leibler divergence from h to q_k , \mathbb{L}^5 the set of logistic-normal distributions on \mathbb{S}^5 . It is shown in the online supplementary materials A.1. that $H_k(\mathbf{p}_i | \boldsymbol{\beta}_k) = \text{Logit-Norm}(\boldsymbol{\mu}_k, \boldsymbol{\Sigma}_k)$, where

$$\boldsymbol{\mu}_k = \mathbb{E}_{q_k} \left[\log \left(\frac{\mathbf{x}_{-6}}{x_6} \right) \right], \quad \boldsymbol{\Sigma}_k = \mathbb{V}_{q_k} \left[\log \left(\frac{\mathbf{x}_{-6}}{x_6} \right) \right],$$

which are available in closed form by the properties of the exponential family. In this scenario, DTMM is not the correct model, but we expect that it is not severely misspecified. Three signal levels are considered with $\alpha = 3, 6, 9$.

IV. **Logistic-normal kernel (single node).** In this scenario, we let $H_k(\mathbf{p}_i | \boldsymbol{\beta}_k) = \text{Logit-Norm}(\boldsymbol{\mu}_k, \boldsymbol{\Sigma}_k)$, where $\boldsymbol{\Sigma}_k = \text{diag}(0.05, 0.05, 1, 1, 1)$, $\boldsymbol{\mu}_1 = (3, 1, a, b, 0)$, $\boldsymbol{\mu}_2 = (2.43, 2.43, a, b, 0)$ and $\boldsymbol{\mu}_3 = (1, 3, a, b, 0)$. The $\boldsymbol{\mu}_k$'s are chosen such that only node C in \mathcal{T}_6 is relevant for clustering. The diagonal covariance matrix suggests that DTMM is misspecified (in comparison, in III the covariance matrices are dense). We consider three signal levels with $(a, b) = (5, 3), (2, 2)$ and $(1, 1)$. Note that when the relative abundance of OTU₃ and OTU₄ are high, the compositional nature of the data implies that fewer counts are generated for OTU₁ and OTU₂ that determine the clustering, resulting in a low signal-to-noise ratio.

V. **Logistic-normal kernel (multiple nodes)**. Similar to scenario IV, we let $H_k(\mathbf{p}_i | \boldsymbol{\beta}_k) = \text{Logit-Norm}(\boldsymbol{\mu}_k, \boldsymbol{\Sigma}_k)$, where $\boldsymbol{\Sigma}_k = \text{diag}(1, 1, 0.05, 0.05, 0.05)$, $\boldsymbol{\mu}_1 = (c, d, 3.5, 3, 2.5)$, $\boldsymbol{\mu}_2 = (c, d, 2.5, 3.5, 3)$ and $\boldsymbol{\mu}_3 = (c, d, 3, 2.5, 3.5)$. In this case, the $\boldsymbol{\mu}_k$'s are chosen such that the clusters are determined by the relative abundance of OTU₃, OTU₄ and OTU₅, which are reflected in nodes D, E and F in \mathcal{T}_6 in [Figure 8](#). Three signal levels with $(c, d) = (6, 6), (3, 3)$ and $(1, 1)$ are considered.

| Kernel | Signal | | $\boldsymbol{\beta}_k$ | |
|--------|--------|----------------|---|--|
| | Level | Parameter | | |
| I DT | W | $\alpha = 1$ | | |
| | M | $\alpha = 3$ | | |
| | S | $\alpha = 6$ | | |
| II Dir | W | $\alpha_0 = 1$ | $\boldsymbol{\alpha}_1 = (2, 2, 5, 2, 3, 1) \cdot \alpha_0$ | |
| | M | $\alpha_0 = 3$ | $\boldsymbol{\alpha}_2 = (2, 4, 3, 2, 1, 3) \cdot \alpha_0$ | |
| | S | $\alpha_0 = 6$ | $\boldsymbol{\alpha}_3 = (2, 6, 1, 2, 2, 2) \cdot \alpha_0$ | |
| III LN | W | $\alpha = 3$ | $q_k = \text{DT}_{\mathcal{T}_6}(\boldsymbol{\nu}_k; \alpha; 0.5)$ | $\boldsymbol{\mu}_k = \mathbb{E}_{q_k} \left[\log \left(\frac{\mathbf{x}_{-6}}{x_6} \right) \right]$ |
| | M | $\alpha = 6$ | $\boldsymbol{\nu}_1 = (10\alpha, 2\alpha)$ | $\boldsymbol{\Sigma}_k = \mathbb{V}_{q_k} \left[\log \left(\frac{\mathbf{x}_{-6}}{x_6} \right) \right]$ |
| | S | $\alpha = 9$ | $\boldsymbol{\nu}_2 = (6\alpha, 6\alpha)$ $\boldsymbol{\nu}_3 = (2\alpha, 10\alpha)$ | |
| IV LN | W | $a = 5, b = 3$ | $\boldsymbol{\mu}_1 = (3, 1, a, b, 0)$ | $\boldsymbol{\Sigma}_{1,2,3} = \begin{pmatrix} 0.05 & & & & \\ & 0.05 & & & \\ & & 1 & & \\ & & & 1 & \\ & & & & 1 \end{pmatrix}$ |
| | M | $a = 2, b = 2$ | $\boldsymbol{\mu}_2 = (2.43, 2.43, a, b, 0)$, | |
| | S | $a = 1, b = 1$ | $\boldsymbol{\mu}_3 = (1, 3, a, b, 0)$ | |
| V LN | W | $c = 6, d = 6$ | $\boldsymbol{\mu}_1 = (c, d, 3.5, 3, 2.5)$ | $\boldsymbol{\Sigma}_{1,2,3} = \begin{pmatrix} 1 & & & & \\ & 1 & & & \\ & & 0.05 & & \\ & & & 0.05 & \\ & & & & 0.05 \end{pmatrix}$ |
| | M | $c = 3, d = 3$ | $\boldsymbol{\mu}_2 = (c, d, 2.5, 3.5, 3)$, | |
| | S | $c = 1, d = 1$ | $\boldsymbol{\mu}_3 = (c, d, 3, 2.5, 3.5)$ | |

Table 2: Mixture kernels for generating the simulated datasets.

Mixture kernels for generating datasets in the 5 simulation scenarios are summarized in [Table 2](#). In each scenario, a “null” case is also considered by setting $K = 1$ in the case with the medium signal level. For each (kernel, signal level) combination, we conduct 100 rounds of simulations. For each simulated dataset with $K = 3$, we calculate the following R^2 as a

measure of the strength of the signal (Anderson, 2001):

$$R^2 = \frac{\text{SSW}}{\text{SST}} = \frac{\sum_{k=1}^3 \sum_{i=1}^{N-1} \sum_{j=i+1}^N d_{\text{BC}}(\mathbf{y}_i, \mathbf{y}_j)^2 \epsilon_{ij}^k / n_k}{\sum_{i=1}^{N-1} \sum_{j=i+1}^N d_{\text{BC}}(\mathbf{y}_i, \mathbf{y}_j)^2 / n},$$

where $d_{\text{BC}}(\cdot, \cdot)$ is the Bray-Curtis dissimilarity, n_k the number of samples in cluster k , $\epsilon_{ij}^k = 1$ if the samples i and j are both in cluster k and 0 otherwise. The average R^2 's of the 100 simulated datasets in each experiment are reported in Table 3 and Table 4.

In each simulation round, we run the Gibbs sampler for DTMM for 2000 iterations and discard the first half of the chain as burn-in. The priors and hyper-parameters for DTMM are set to the recommended choice in Section 2.3. The initial values for the clustering labels in the Markov chain are set to the labels of running the k -means algorithm with $k = 5$. For DTMM, we output \mathbf{c}_{LS} as a representative clustering. For PAM and Hclust, we use the Bray-Curtis dissimilarity on the relative abundance as the underlying distance measure between samples. For all competitors other than DMM, the number of clusters is required as a tuning parameter, we set this parameter to the truth 3 when running these methods.

3.1.2 Analyses

To compare the performance of different methods, we compute the Jaccard index (Jaccard, 1912) between the clusters obtained by each method and the truth. For a specific clustering \mathbf{c} and the true clustering \mathbf{c}_0 , the Jaccard index between \mathbf{c} and \mathbf{c}_0 is defined as $J(\mathbf{c}, \mathbf{c}_0) = \mathcal{N}_{\mathbf{c} \cap \mathbf{c}_0} / \mathcal{N}_{\mathbf{c} \cup \mathbf{c}_0}$, where $\mathcal{N}_{\mathbf{c} \cap \mathbf{c}_0}$ is the number of pairs of samples that are in the same cluster under both \mathbf{c} and \mathbf{c}_0 , $\mathcal{N}_{\mathbf{c} \cup \mathbf{c}_0}$ the number of pairs of samples that are in the same cluster under at least one of \mathbf{c} and \mathbf{c}_0 . When \mathbf{c} gives the same clustering as \mathbf{c}_0 , $J(\mathbf{c}, \mathbf{c}_0) = 1$. In each simulation scenario, we compare the root mean squared error of each method m : $\text{RMSE}^{(m)} = \sqrt{\sum_{r=1}^{100} [J(\mathbf{c}_r^{(m)}, \mathbf{c}_0) - 1]^2 / 100}$, where $\mathbf{c}_r^{(m)}$ is the clustering obtained by method m in simulation round r . As some references, let $\mathbf{c}_0 = (1 \cdot \mathbf{1}_{40}^\top, 2 \cdot \mathbf{1}_{30}^\top, 3 \cdot \mathbf{1}_{20}^\top)$, $\mathbf{c}_1 = (1 \cdot \mathbf{1}_{90}^\top)$, $\mathbf{c}_2 = (1 \cdot \mathbf{1}_{30}^\top, 2 \cdot \mathbf{1}_{30}, 3 \cdot \mathbf{1}_{30})$ and $\mathbf{c}_3 = (1 \cdot \mathbf{1}_{40}^\top, 2 \cdot \mathbf{1}_{50})$, where $\mathbf{1}_n$ is the n -dimensional vector with all element equal to 1. We have $\sqrt{[J(\mathbf{c}_1, \mathbf{c}_0) - 1]^2} = 0.65$, $\sqrt{[J(\mathbf{c}_2, \mathbf{c}_0) - 1]^2} = 0.50$ and $\sqrt{[J(\mathbf{c}_3, \mathbf{c}_0) - 1]^2} = 0.30$. Table 3 and Table 4 shows the RMSE of DTMM and the competitors under all simulation scenarios. Boxplots of the Jaccard index reported by each method are shown in Figure S1 and Figure S2 in the online supplementary materials A.2.

When $K = 3$, DTMM is always one of the top two methods under comparison. When it's not the best method, its performance is often close to the best. Without utilizing the information provided by the phylogenetic tree, all competitors of DTMM provide limited insights on the clustering when the signal is weak or medium. Moreover, these competitors rely on global distance measures between samples and treat the six OTUs equivalently. As a result, in scenario like I and IV where the signal is local to a single internal node of the phylogenetic tree, these methods have poor performance. Even in scenario V where half

| | | $n = 90$ | | | | | | | |
|------|-------|----------|------|-------------|-------------|------|--------|------|------|
| Expt | Level | Signal | | Method | | | | | |
| | | R^2 | DTMM | DMM | K-ms | PAM | Hclust | Spec | |
| I | DT | – | – | 0.43 | 0.51 | – | – | – | – |
| | | W | 0.30 | 0.56 | 0.64 | 0.67 | 0.71 | 0.65 | 0.71 |
| | | M | 0.35 | 0.33 | 0.65 | 0.69 | 0.69 | 0.64 | 0.71 |
| | | S | 0.37 | 0.17 | 0.65 | 0.69 | 0.71 | 0.65 | 0.70 |
| II | Dir | – | – | 0.35 | 0.00 | – | – | – | – |
| | | W | 0.35 | 0.53 | 0.53 | 0.55 | 0.59 | 0.58 | 0.57 |
| | | M | 0.52 | 0.18 | 0.30 | 0.37 | 0.33 | 0.37 | 0.33 |
| | | S | 0.60 | 0.04 | 0.09 | 0.32 | 0.19 | 0.38 | 0.22 |
| III | LN-A | – | – | 0.46 | 0.06 | – | – | – | – |
| | | W | 0.37 | 0.49 | 0.64 | 0.53 | 0.53 | 0.54 | 0.54 |
| | | M | 0.38 | 0.23 | 0.64 | 0.50 | 0.46 | 0.55 | 0.47 |
| | | S | 0.39 | 0.10 | 0.64 | 0.48 | 0.44 | 0.53 | 0.46 |
| IV | LN-S | – | – | 0.60 | 0.54 | – | – | – | – |
| | | W | 0.10 | 0.35 | 0.72 | 0.77 | 0.78 | 0.73 | 0.74 |
| | | M | 0.41 | 0.21 | 0.54 | 0.59 | 0.54 | 0.60 | 0.53 |
| | | S | 0.60 | 0.17 | 0.37 | 0.36 | 0.24 | 0.41 | 0.27 |
| V | LN-M | – | – | 0.41 | 0.61 | – | – | – | – |
| | | W | 0.04 | 0.20 | 0.78 | 0.78 | 0.79 | 0.78 | 0.76 |
| | | M | 0.23 | 0.14 | 0.65 | 0.76 | 0.70 | 0.74 | 0.68 |
| | | S | 0.53 | 0.17 | 0.49 | 0.22 | 0.20 | 0.39 | 0.22 |

Table 3: RMSE of the Jaccard index (small sample size). Cells with the lowest RMSE in each row are highlighted.

of the OTUs are relevant for clustering, these methods still suffer unless the signal is very strong. In scenario II where the signal is global, all methods perform reasonably well. Note that in this scenario, DTMM can outperform DMM when $n = 90$ even the latter is the true model. This is because DMM relies on a Laplace approximation to a six dimensional integral when computing the marginal likelihoods to choose the number of clusters. When the sample size is small, DMM tends to choose less than three clusters due to the poor approximation. When $n = 180$, DMM is more likely to choose the right number of clusters even with the inaccurate approximation. Thus the performance of DMM improves significantly with more samples. Our experience suggests that DMM tends to underestimate the number of clusters in most cases. For example, in scenario I and III, DMM simply puts all samples in a same cluster when $n = 90$.

In our simulation settings, there are two factors that determine the effect of the increase

| | | $n = 180$ | | | | | | | |
|------|--------|-----------|--------|-------------|-------------|------|-------------|------|------|
| Expt | Signal | | Method | | | | | | |
| | Level | R^2 | DTMM | DMM | K-ms | PAM | Hclust | Spec | |
| I | DT | – | – | 0.38 | 0.75 | – | – | – | – |
| | | W | 0.30 | 0.45 | 0.65 | 0.67 | 0.72 | 0.65 | 0.71 |
| | | M | 0.35 | 0.36 | 0.69 | 0.69 | 0.72 | 0.66 | 0.71 |
| | | S | 0.36 | 0.19 | 0.72 | 0.69 | 0.71 | 0.65 | 0.70 |
| II | Dir | – | – | 0.50 | 0.00 | – | – | – | – |
| | | W | 0.34 | 0.51 | 0.46 | 0.58 | 0.59 | 0.59 | 0.56 |
| | | M | 0.51 | 0.16 | 0.12 | 0.33 | 0.29 | 0.37 | 0.28 |
| | | S | 0.59 | 0.08 | 0.04 | 0.31 | 0.17 | 0.39 | 0.22 |
| III | LN-A | – | – | 0.67 | 0.21 | – | – | – | – |
| | | W | 0.37 | 0.56 | 0.55 | 0.52 | 0.48 | 0.56 | 0.51 |
| | | M | 0.38 | 0.26 | 0.55 | 0.49 | 0.40 | 0.56 | 0.44 |
| | | S | 0.39 | 0.13 | 0.56 | 0.46 | 0.38 | 0.54 | 0.41 |
| IV | LN-S | – | – | 0.74 | 0.66 | – | – | – | – |
| | | W | 0.09 | 0.62 | 0.75 | 0.77 | 0.78 | 0.72 | 0.73 |
| | | M | 0.40 | 0.46 | 0.52 | 0.58 | 0.54 | 0.62 | 0.47 |
| | | S | 0.59 | 0.19 | 0.33 | 0.34 | 0.22 | 0.42 | 0.20 |
| V | LN-M | – | – | 0.48 | 0.69 | – | – | – | – |
| | | W | 0.03 | 0.29 | 0.81 | 0.79 | 0.79 | 0.78 | 0.78 |
| | | M | 0.22 | 0.24 | 0.73 | 0.76 | 0.71 | 0.74 | 0.57 |
| | | S | 0.52 | 0.17 | 0.25 | 0.17 | 0.17 | 0.24 | 0.17 |

Table 4: RMSE of the Jaccard index (large sample size). Cells with the lowest RMSE in each row are highlighted.

of sample size on the performance of the two model-based clustering methods. On the one hand, since more samples are available per cluster, the models have a better chance to capture the cluster centroids well once they identify the correct number of clusters. On the other hand, more samples makes it harder to get the number of clusters right. These two fighting forces together determine the overall performance shift of the two model-based methods, yet which force prevails is unclear. For DTMM, when the model is mis-specified (as in scenarios III, IV and V), the model tends to identify too many small clusters, resulting in a worse overall performance. For the distance-based clustering methods, these two factors play no role since we assume that the number of clusters is known. In general, our observations suggest that these methods benefit a little from more samples when the signal is strong. Among the distance-based methods, PAM and Spec have a better overall performance. We thus recommend using these two methods to help choose the initial values of the MCMC

chain of DTMM.

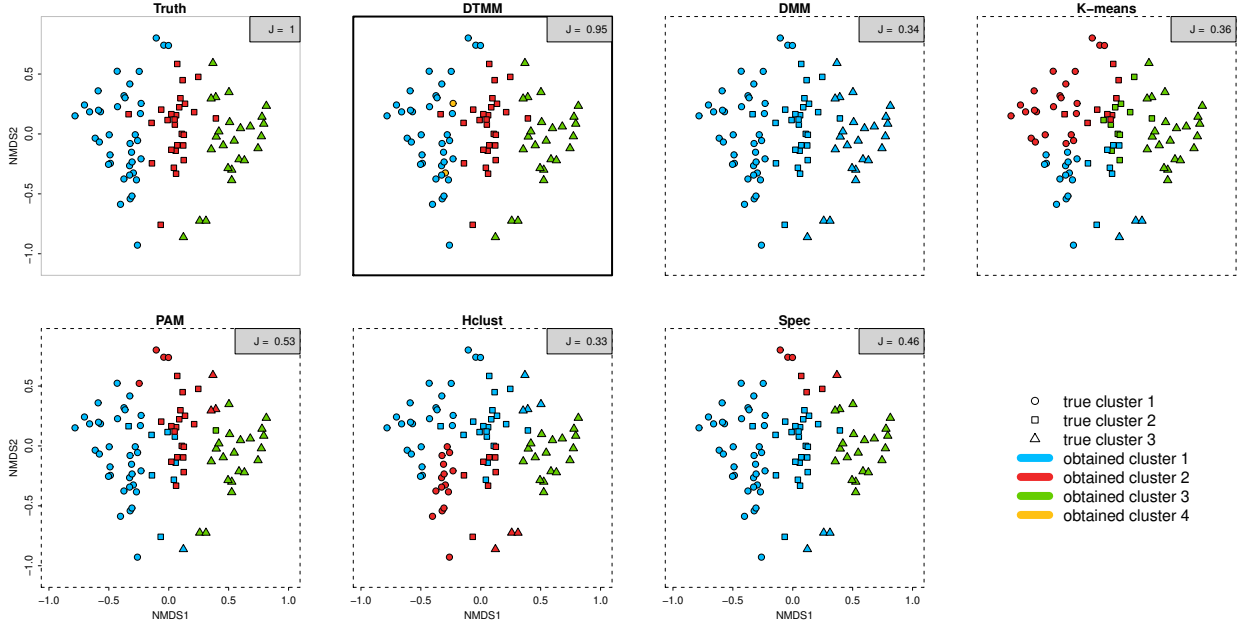


Figure 10: 2D NMDS plot of samples in a simulation round in scenario IV ($n = 90$, medium noise level). In each sub-plot, the true clustering is indicated by the shape of the points while the clustering obtained is indicated by the color.

We next zoom in to an example to further study the properties of DTMM. In this example, we consider a specific simulation round in scenario IV with the medium noise level ($n = 90$). **Figure 10** shows the 2D NMDS plot of the samples colored by the clustering obtained by each method. In this example, the clustering is roughly determined only by the first NMDS axis. By utilizing the information provided by the phylogenetic tree, DTMM is capable of picking the relevant dimensions and clustering efficiently. As for a representative clustering, DTMM finds 4 clusters, with one falsely identified cluster containing only two samples. This is consistent with the well-known fact that inference based on Dirichlet process mixture models can identify small clusters that do not reflect the true data-generating process ([Miller and Harrison, 2013](#)). One feature that differs DTMM from its competitors is that it not only outputs a representative clustering, but also a whole MCMC trajectory that allows natural uncertainty quantifications. **Figure 11** (a) shows the probability of two samples being clustered together by DTMM. Clearly, three stable clusters are identified. Although DTMM falsely puts the first two samples in a separate cluster, the uncertainty is large. There is a high probability that these two samples are actually from the second cluster. The estimated centroids for the three large clusters obtained by DTMM have compositions $(0.44, 0.05, 0.23, 0.22, 0.03, 0.03)$, $(0.24, 0.25, 0.23, 0.22, 0.03, 0.03)$ and $(0.08, 0.41, 0.23, 0.22, 0.03, 0.03)$. In comparison, the centroids' compositions in the true data-generating process are $(0.51, 0.07, 0.19, 0.19, 0.03, 0.03)$, $(0.29, 0.29, 0.19, 0.19, 0.03, 0.03)$

and (0.07, 0.51, 0.19, 0.19, 0.03, 0.03), respectively. A byproduct of DTMM is its ability to perform node selection during the clustering procedure. **Figure 11** (b) shows the relative abundance of the samples as well as the estimated posterior node selection probabilities. In this example, DTMM is able to uncover the correct subset of internal nodes that are relevant for clustering. We also consider an example from simulation scenario V. Illustrations similar to **Figure 10** and **Figure 11** can be found in **Figure S3** and **Figure S4** in the online supplementary materials A.2.

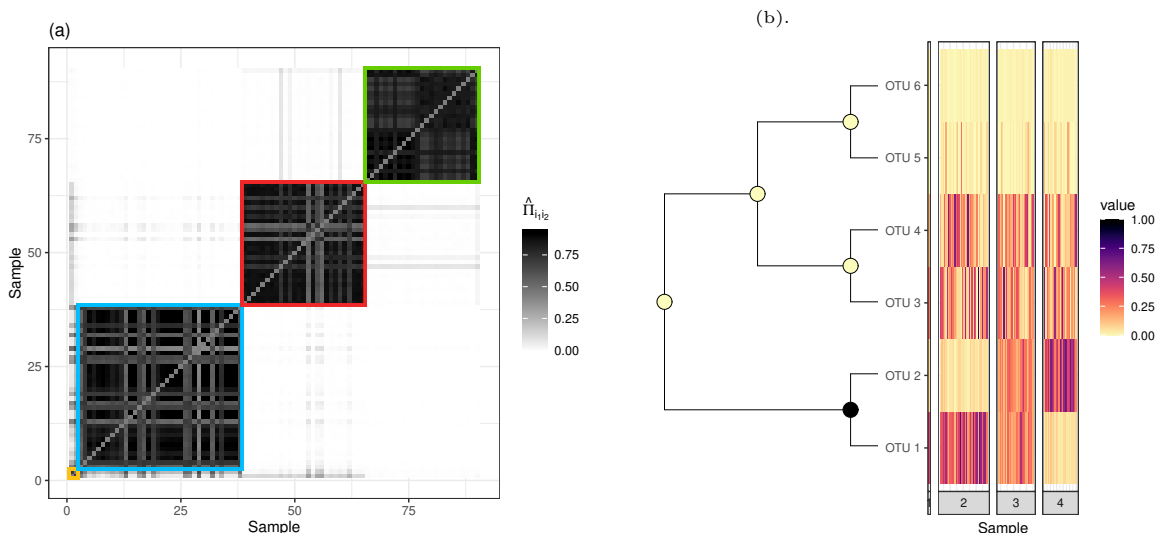


Figure 11: Illustrations for an example from simulation scenario IV. (a): Probability of two samples being clustered together by DTMM based on 1000 post-burnin MCMC samples. The samples are ordered by their cluster labels from DTMM. The clusters identified by DTMM are highlighted by squares colored as in **Figure 10**. (b): An illustration of the node selection property of DTMM. The nodes are colored by their estimated posterior node selection probabilities. The heatmap plots the relative abundance of the samples grouped by their cluster labels from DTMM.

3.2 Validation

Validating the results of unsupervised learning is often challenging. In microbiome clustering analyses, the best practice is to check the resulting clusters with scientists to see if they provide any biological insights on a case by case basis. In this section, instead of trying to provide a general solution of how to justify the clusters found by DTMM, we provide an example to show that DTMM can identify biologically meaningful clusters in real microbiome applications.

Specifically, we reanalyze the data in [Dethlefsen and Relman \(2011\)](#), which studies the responses of stable gut microbiota to antibiotic disturbance. In this study, the distal gut microbiome of three patient (patient D, E and F) were monitored over 10 months, including

two 5-day antibiotic treatment courses separated by a 5-month interim period. 52 to 56 samples were collected for each patient in the experiment. For example, samples of patient D and F are shown in Figure 12 and Figure 13. These figures also illustrate the design of the study. In our analyses, the OTU counts are aggregated to the genus level, which gives 59 OTUs (genus) in total.

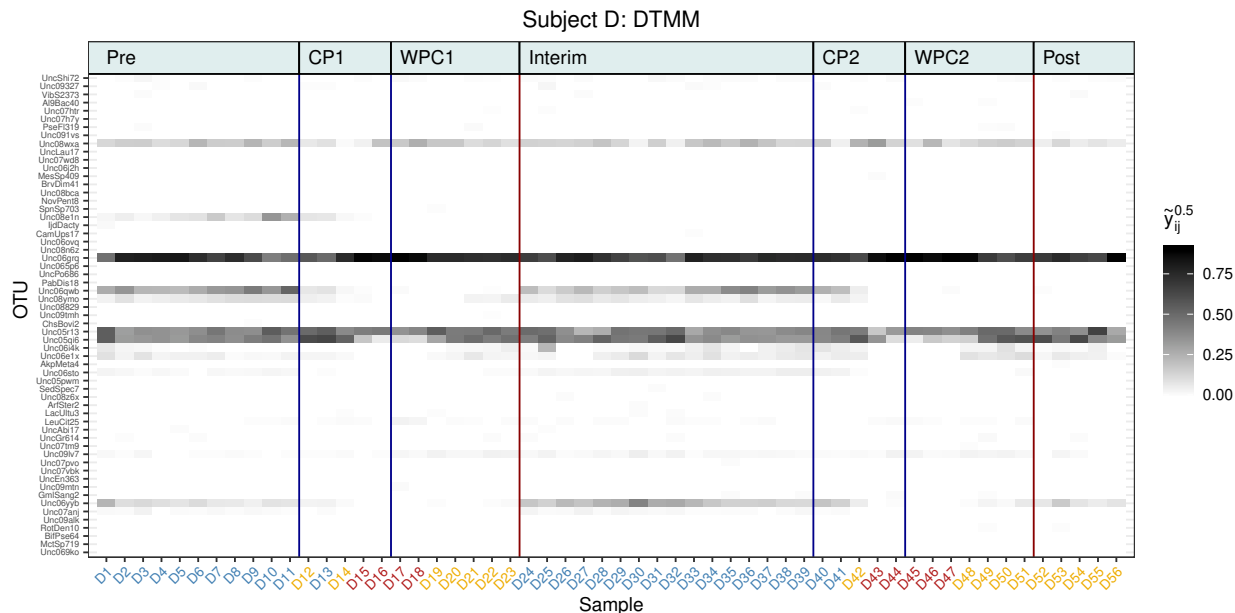


Figure 12: The heatmap of the microbiome samples of patient D (after the square-root transform). Each column represents a specific sample. The columns are ordered by the times the samples were collected. The colors of the x -axis labels represent the clustering labels of the samples returned by DTMM. The blue vertical lines mark the two antibiotic treatment courses. “CP” denotes the antibiotic treatment (ciprofloxacin); “WPC” is the week post treatment; “Pre” and “Post” denote the pre-treatment and post-treatment period, respectively.

We analyze the samples from the three patients separately. For each patient, we ignore the time information of when the samples were taken and run DTMM on these samples for 2500 iterations. The first half of the chain was discarded as burn-in. The clustering results for patient D and F are shown in Figure 12 and Figure 13 (the x -axis labels in these plots are colored by the cluster labels in C_{LS} of the samples they represent). For patient D, DTMM identifies three clusters, which can be interpreted as the *stable*, *sterile* and *recover* stages of the microbiota. Based on the clustering results, the gut microbiota of patient D was stable before the treatment. It was able to recover to some stable states from antibiotic treatment within a week after the treatment was finished. However, although the microbiota was able to fully recover to the pre-treatment state after the first antibiotic treatment course, it never made a full recovery to the original state after the second (repeated) antibiotic treatment.

For patient F, DTMM identifies four clusters corresponding to the *stable 1* (blue), *sterile*, *recover* and *stable 2* (purple) stages, respectively. Like patient D, the gut microbiota of patient F was stable before the treatment and was able to recover from the treatments. Unlike patient D, it did not recover to the pre-treatment state even after the first treatment course. Moreover, it took longer for patient F to recover than patient D. We note that these findings are all consistent to the findings in [Dethlefsen and Relman \(2011\)](#), where the time and design information was used to get these results. Therefore, the clusters found by DTMM are biologically interpretable in this example.

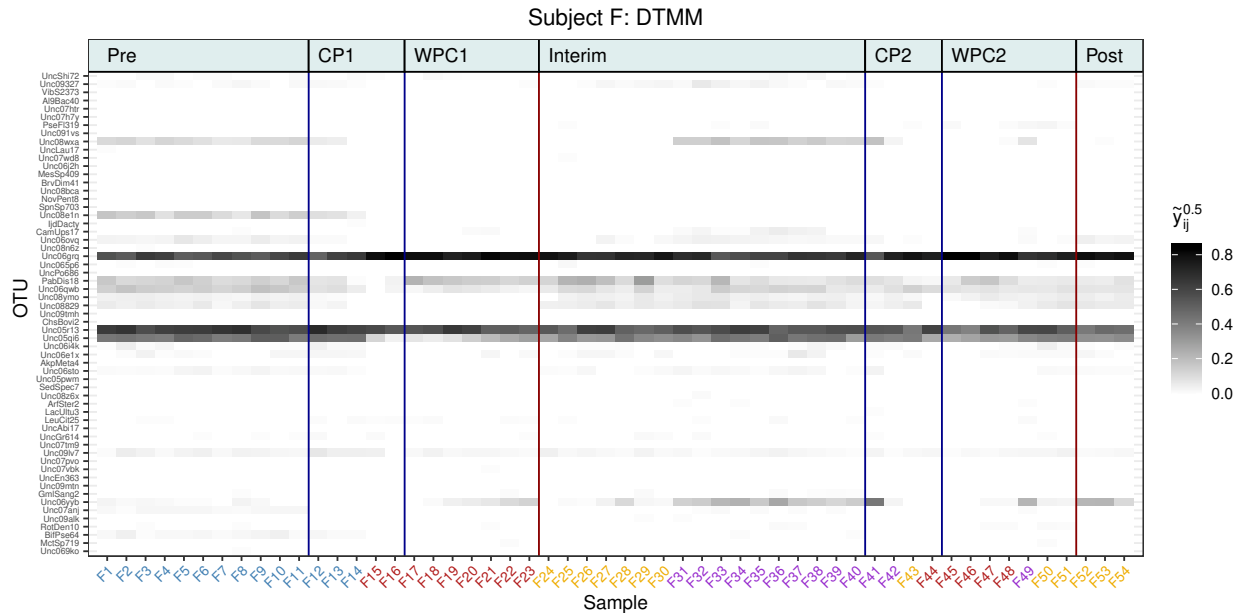


Figure 13: The heatmap of the microbiome samples of patient F (after the square-root transform). Each column represents a specific sample. The columns are ordered by the times the samples were collected. The colors of the x -axis labels represent the clustering labels of the samples returned by DTMM. The legends are defined the same way as in [Figure 12](#).

As a comparison, the clustering results for these two patients under DMM are shown in [Figure S5](#) and [Figure S6](#) in the online supplementary materials A.2. For both patients, DMM returns two clusters with high probability, with the two clusters roughly representing the *stable* and *unstable* stages of the microbiota, respectively. In this example, DTMM is able to discover more interesting latent structures among samples than DMM. It is worth noting that in each analysis, microbiome samples were collected from the same patient. Thus the level of cross-sample variations in this study is much smaller than microbiome studies with multiple subjects. In those cases, we expect DTMM to benefit more from its improved flexibility over DMM and discover even more interpretable structures than the latter.

4 Case studies

The American Gut project (McDonald et al., 2015, 2018) aims at building an open-source and open-access reference microbiome dataset for general scientific use based on 16S rRNA sequencing and the QIIME pipeline (Caporaso et al., 2010). It collects mouth, skin and feces samples over a large variety of US participants on a voluntary basis. The participants send their microbiome samples to UC San Diego for sequencing and complete a questionnaire that covers the dietary habits, lifestyle, and health history.

In this section, we apply DTMM to the July 2016 version of the fecal data from the American Gut Project to construct enterotypes for two groups of samples: firstly, we consider participants who have been diagnosed with inflammatory bowel disease (IBD); secondly, we consider participants who have been diagnosed with diabetes. The diagnoses are made by a medical professional (a doctor or a physician assistant). The specific version of the American Gut dataset contains an OTU table of 27774 OTUs. We focus on the top 75 OTUs based on total counts to reduce noises in the dataset and control for the sequencing errors. The top 75 OTUs on average retain 2/3 of the total counts in a sample. We filter the samples by only considering participants with at least 500 counts on the top 75 OTUs. This filtering ends up with 189 samples diagnosed with IBD and 106 samples diagnosed with diabetes that we use in our analysis.

In the following sections, we fit DTMM to each of the two datasets with the priors and hyperparameters set to the recommended choices in Section 2.3. In each analysis, we run the Gibbs sampler in Section 2.4 for 5000 iterations and discard the first half of the chain as burn-in. The cluster labels are initiated by running the PAM algorithm with $K = 5$.

Key findings from our analyses are summarized as follows:

- The enterotypes (clusters) are determined by a large number of OTUs jointly in a sophisticated manner instead of by a few OTUs.
- OTUs from genera *Bacteroides*, *Prevotella* and *Ruminococcus* are typically important in identifying enterotypes, which is consistent to the findings in previous works (Arumugam et al., 2011).
- The number of enterotypes and the OTUs that characterize each enterotype can differ across datasets.
- DMM tends to find larger clusters that are unions of clusters found by DTMM.

4.1 IBD

We first consider samples from participants that are diagnosed with IBD. Figure 14 shows the traceplots of some one dimensional parameters or summaries of the posterior samples. The Markov chain stabilizes and mixes reasonably well after about 750 iterations. Figure 14 (a) and Figure 14 (b) show the traceplots of the Dirichlet process precision parameter β and the prior global coupling probability λ . The posterior means of these parameters are 0.87

and 0.53, respectively. Traceplot of the sampled number of internal nodes with $\gamma(A) = 1$ is shown in [Figure 14](#) (c). On average, 39 out of 74 nodes are marked as relevant to the clustering process, indicating that the clustering process is determined by various OTUs jointly in a complicated way instead of being dominated by a few OTUs that are dominant in terms of counts. [Figure 14](#) (d) shows the cumulative proportion of samples in the largest one, two, three, four and five clusters for each iteration. DTMM tends to assign samples into 5 clusters.

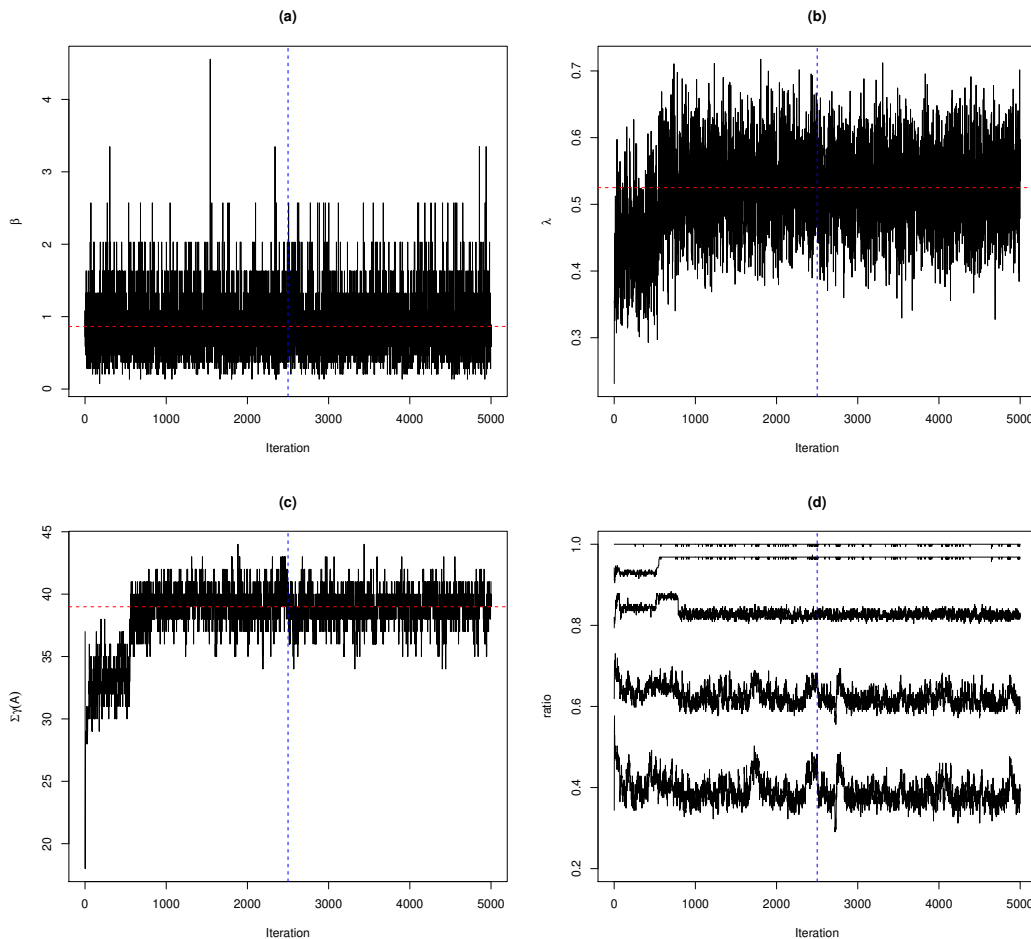


Figure 14: Traceplots of some summary statistics.

We find \mathcal{C}_{LS} as defined in (2.30), which corresponds to $\mathbf{c}^{(t_0)}$ with $t_0 = 2717$. \mathcal{C}_{LS} assigns the samples into five clusters, with size 6, 41, 73, 42 and 27, respectively. The estimated centroids of the five clusters are shown in [Figure 15](#). [Figure 15](#) also shows the estimated posterior means of the coupling indicator $s(A)$ at $A \in \mathcal{I}$. Most internal nodes that are irrelevant to clustering are close to the leaves of the tree. Nodes that are more “global” (have more descendant OTUs) generally contribute to the clustering. This indicates that the

clustering process is determined by most OTUs jointly in a complicated manner. **Figure 16** (left) shows the estimated pairwise clustering probability matrix $\hat{\Pi}$ with the rows and columns ordered by the labels in \mathbf{C}_{LS} . There are noticeable uncertainties in the clustering, especially between cluster 2, 3 and 4. This can also be seen from **Figure 16** (right), where we plot the heatmap of the samples (after the square-root transform) grouped by their labels in \mathbf{C}_{LS} . Clearly, clusters 2, 3 and 4 are similar. **Figure 16** (right) also shows that the within-cluster variations among samples are large.

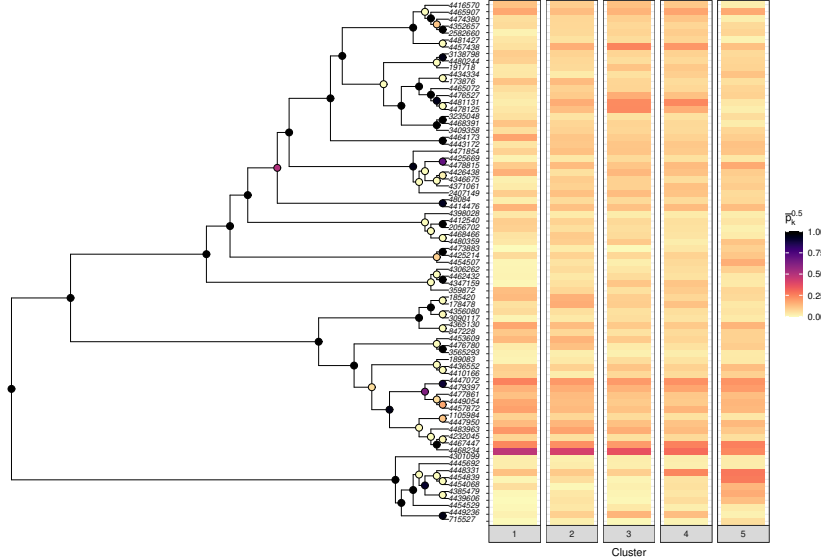


Figure 15: Left: Estimated posterior means of the coupling indicators at each node of the phylogenetic tree. Right: The estimated centroids of the five clusters in \mathbf{C}_{LS} (after the square-root transform).

To see which OTUs are more important in determining \mathbf{C}_{LS} , we consider the following heuristic measure of OTU importance: for $1 \leq j \leq M$, let

$$\vartheta_j = \frac{SSB_j}{SSW_j} = \frac{\sum_{c \in \mathbf{C}_{LS}} n_c (\bar{y}_{cj} - \bar{y}_j)^2}{\sum_{c \in \mathbf{C}_{LS}} \sum_{c_i=c} (y_{ij} - \bar{y}_{cj})^2}, \quad (4.1)$$

where \bar{y}_j is the overall mean of y_{ij} , \bar{y}_{cj} the mean of y_{ij} for samples with $c_i = c$. **Table 5** shows the top 10 OTUs in determining \mathbf{C}_{LS} in terms of ϑ_j as well as their compositions in each cluster centroid. Overall, \mathbf{C}_{LS} is jointly determined by multiple OTUs in a complicated way. Note that OTUs that are important for clustering are not necessarily those with abundant counts. For example, OTU-4468234 and OTU-4447072 (both are *Bacteroides*) are the two OTUs with the most counts in the dataset. However, these two OTUs are prevalent in most samples and thus have limited roles in the clustering.

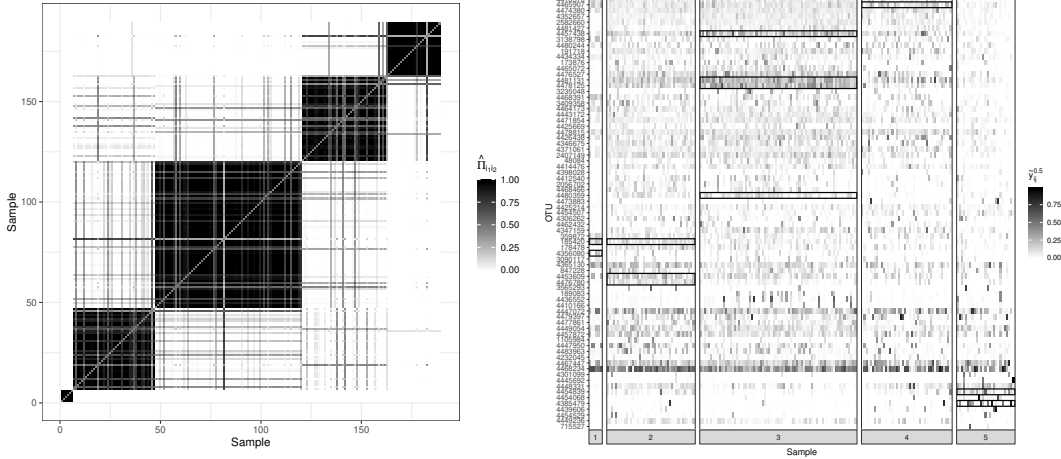


Figure 16: Left: Estimated pairwise co-clustering probabilities. Right: Heatmap of the samples (after the square-root transform) grouped by their labels in \mathcal{C}_{LS} . The black boxes illustrate the characteristic OTUs of each cluster.

We next compare the five resulting clusters in more details. [Figure 17](#) shows the boxplot of the Shannon diversity of samples in the five clusters, respectively. Samples from cluster 2 and 3 tend to have more evenly distributed counts across OTUs compared to those from cluster 1 and 5. Similar to (4.1), we can define a heuristic measure of OTU importance in characterizing each of the five clusters. Specifically, for $c = 1, \dots, 5$, let

$$\vartheta_j^c = \frac{SSB_j^c}{SSW_j^c} = \frac{n_c(\bar{y}_{cj} - \bar{y}_j)^2 + n_{-c}(\bar{y}_{-cj} - \bar{y}_j)^2}{\sum_{c_i=c} (y_{ij} - \bar{y}_{cj})^2 + \sum_{c_i \neq c} (y_{ij} - \bar{y}_{-cj})^2}, \quad (4.2)$$

where n_{-c} is the number of samples that are not in cluster c , \bar{y}_{-cj} the mean of y_{ij} for samples with $c_i \neq c$. (4.2) is equivalent to merging the four clusters other than cluster c in (4.1). The boxes in [Figure 16](#) (right) indicate the top OTUs in terms of ϑ_j^c for each c (only OTUs with $\vartheta_j^c > 0.1$ are shown).

Based on these results, we can characterize each cluster by a few OTUs with the top ϑ_j^c . For example, samples from cluster 2 tend to have more counts from the *Rikenellaceae* family (represented by OTU-4453609 and OTU-4476780). Cluster 3 is characterized by having more abundance in the *Faecalibacterium* (represented by OTU-4478125 and OTU-4481131) and the *Lachnospiraceae* family (represented by OTU-4481127 and OTU-4457438). [Arumugam et al. \(2011\)](#) proposed three enterotypes in human gut microbial communities that are characterized by the variation in the levels of one of the three genera: *Bacteroides*, *Prevotella* and *Ruminococcus*. Our analysis suggests that the enterotypes are determined by a more sophisticated mechanism involving more genera. Although OTUs from the *Bacteroides*, *Prevotella* and *Ruminococcus* genera are not always those with the largest ϑ_j^c , they are playing important roles in identifying the five clusters. For example, OTUs from the *Prevotella* genus have large ϑ_j^3 and are thus crucial in determining cluster 3 while OTUs from the *Ruminococcus*

| OTU | Family | Genus | ϑ_j | C1 | C2 | C3 | C4 | C5 |
|---------|--------------------|------------------|---------------|------|------|------|------|------|
| 185420 | Bacteroidaceae | Bacteroides | 0.43 | 2.01 | 2.62 | 0.98 | 0.66 | 0.54 |
| 4478125 | Ruminococcaceae | Faecalibacterium | 0.43 | 0.22 | 1.71 | 5.72 | 2.71 | 0.10 |
| 4356080 | Barnesiellaceae | – | 0.33 | 0.53 | 0.41 | 0.37 | 0.42 | 0.28 |
| 4476780 | Rikenellaceae | – | 0.32 | 0.14 | 1.70 | 0.15 | 0.33 | 1.04 |
| 4453609 | Rikenellaceae | – | 0.26 | 2.08 | 2.43 | 1.15 | 0.71 | 0.85 |
| 4480359 | Ruminococcaceae | – | 0.22 | 0.22 | 1.02 | 1.22 | 0.11 | 1.48 |
| 4465907 | Lachnospiraceae | Blautia | 0.21 | 3.32 | 1.82 | 2.40 | 3.47 | 3.04 |
| 4481131 | Ruminococcaceae | Faecalibacterium | 0.18 | 0.11 | 2.92 | 5.62 | 6.11 | 0.22 |
| 4457438 | Lachnospiraceae | – | 0.19 | 0.36 | 2.72 | 6.43 | 4.67 | 1.68 |
| 4385479 | Enterobacteriaceae | Proteus | 0.17 | 0.02 | 0.21 | 0.04 | 0.24 | 2.91 |

Table 5: Estimated cluster-specific compositions of the top 10 OTUs in determining \mathbf{C}_{LS} in terms of ϑ_j . Values of the OTU compositions are shown in the percentage scale.

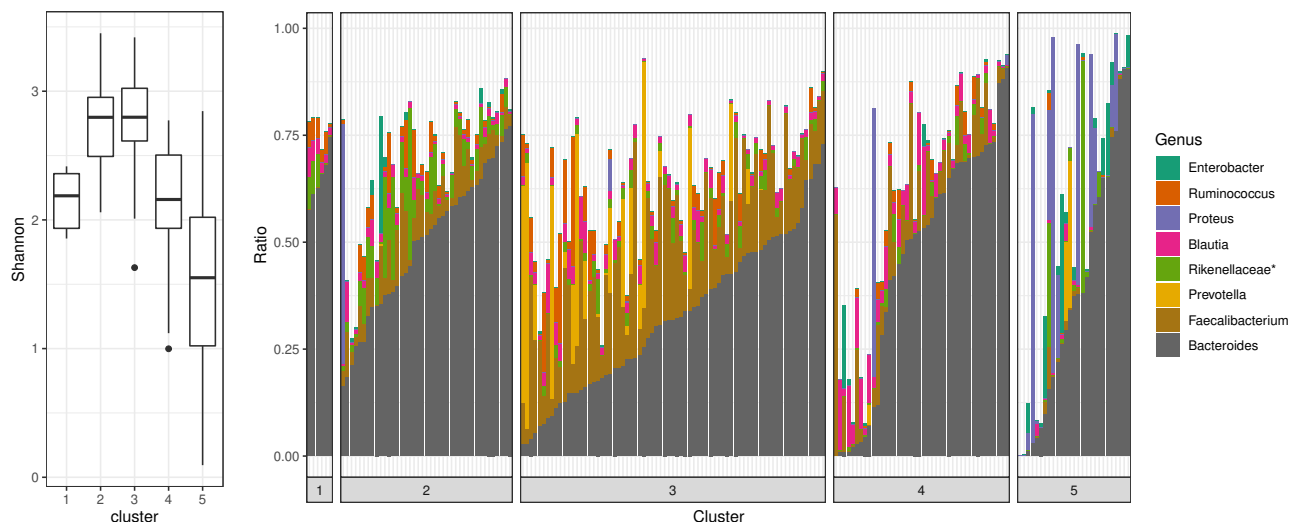


Figure 17: Left: Boxplot of the Shannon diversity of samples in each cluster. Right: Relative abundance of 8 genera for each sample. A genus is chosen if its descendant OTUs have large ϑ_j^c for some c . For the 3 OTUs with unavailable genera information, their family is shown instead (indicated by *Rikenellaceae**).

genus have large ϑ_j^1 and ϑ_j^2 and are thus important in identifying cluster 1 and 2. This can also be seen from [Figure 17](#) (right), where relative abundance of 8 genera picked by ϑ_j^c are shown for each sample. The samples are grouped by their cluster labels in \mathbf{C}_{LS} .

4.2 Diabetes

Similar to Section 4.1 we apply DTMM to samples from participants that are diagnosed with diabetes. Counterparts of Figure 14 and Figure 16 are shown in Figure S7 and Figure S8 in the online supplementary materials C. In this example, DTMM finds three clusters with C_{LS} . Figure 18 shows the estimated centroids of the three clusters as well as the estimated posterior means of the coupling indicators at each node of the phylogenetic tree. Figure 17 (right) shows for each sample the relative abundance of 6 genera selected based on the importance of their descendant OTUs in identifying the three clusters. Compared with the IBD example, the enterotypes in this case can be identified easier. For example, samples in cluster 3 tend to have significantly lower abundance in *Faecalibacterium* and *Bacteroides*, which are the dominating genera in most samples. Compared with cluster 2, cluster 1 is identified with relatively more counts from OTU-173876 and the *Prevotella* family.

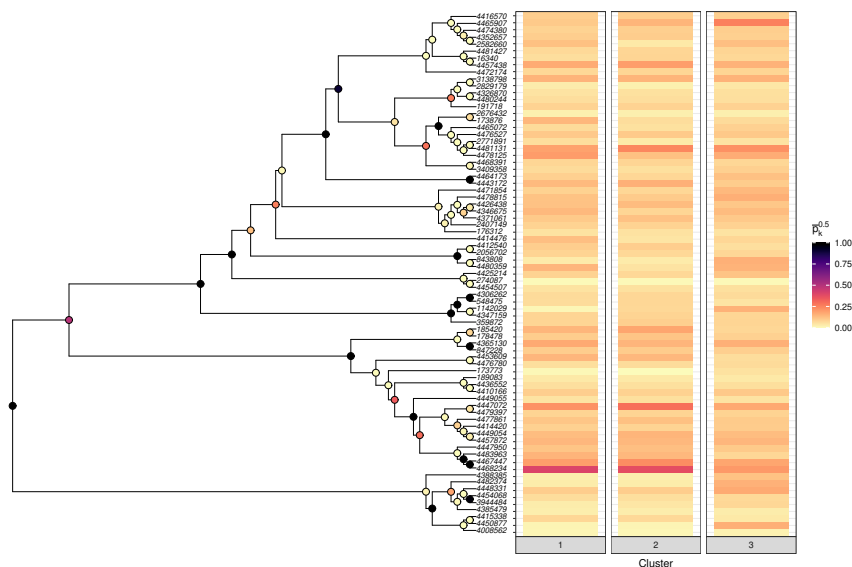


Figure 18: Left: Estimated posterior means of the coupling indicators at each node of the phylogenetic tree. Right: The estimated centroids of the three clusters in C_{LS} (after the square-root transform).

On average, 21 out of 75 internal nodes of \mathcal{T} are estimated as relevant to the clustering process. Compared with the IBD example in Section 4.1, fewer nodes are involved. The reason for this is twofold. Firstly, as we discussed previously, clusters in the diabetes example are determined by fewer OTUs (genera), which is reflected in the number of internal nodes selected. Secondly, as shown in Figure S8 (right), a few OTUs play crucial roles in determining multiple clusters. As a comparison, as shown in Figure 16 (right), each cluster in the IBD example is determined by a unique set of OTUs. Since DTMM marks an internal

node as relevant if it is relevant in determining *any* cluster, more nodes are selected in the IBD example.

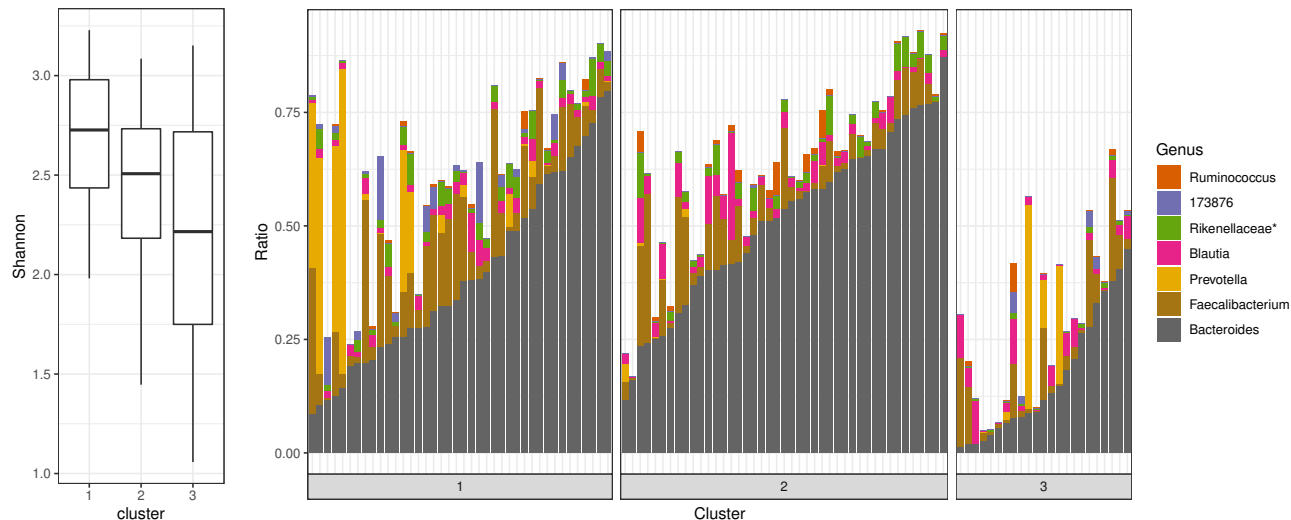


Figure 19: Left: Boxplot of the Shannon diversity of samples in each cluster. Right: Relative abundance of 6 genera for each sample. A genus is chosen if its descendant OTUs have large ϑ_j^c for some c . For the 3 OTUs with unavailable genera information, their family is shown instead (indicated by *Rikenellaceae**). OTU-173876 is important in identifying cluster 1 and is illustrated directly since no genera or family information is available for this OTU.

4.3 DTMM vs. DMM

We also apply DMM to the two examples in this section and compare it with DTMM. DMM reports two clusters in both examples (see Figure S10 in the online supplementary materials C). For the IBD dataset, Figure 20 (left) shows the two-dimensional NMDS plot of the data, colored by the cluster labels reported by DMM. In comparison, Figure 20 (right) shows the same NMDS plot colored by the cluster labels in \mathcal{C}_{LS} reported by DTMM.

The five clusters reported by DTMM can be seen as refinements of the two clusters reported by DMM. Roughly, cluster B identified by DMM is the union of cluster 2 and 3 from DTMM while cluster A found by DMM is the union of cluster 1, 4 and 5 from DTMM. As shown in Figure 16 (right) and Figure 17 (right), those subclusters from DTMM are not differentiated by OTUs with dominant counts. Thus it is very unlikely for DMM to make further splits. Moreover, based on Figure 16 (right), samples within each cluster from DTMM tend to show different levels of heterogeneities across OTUs, making the underlying Dirichlet-multinomial model of DMM unrealistic. For example, counts of OTUs from the *Prevotella* genus tend to show large within cluster variations among samples in cluster 3. To capture this level of variation, DMM has to push the cluster-specific dispersion parameter very large, essentially loose its ability to effectively find those subclusters.

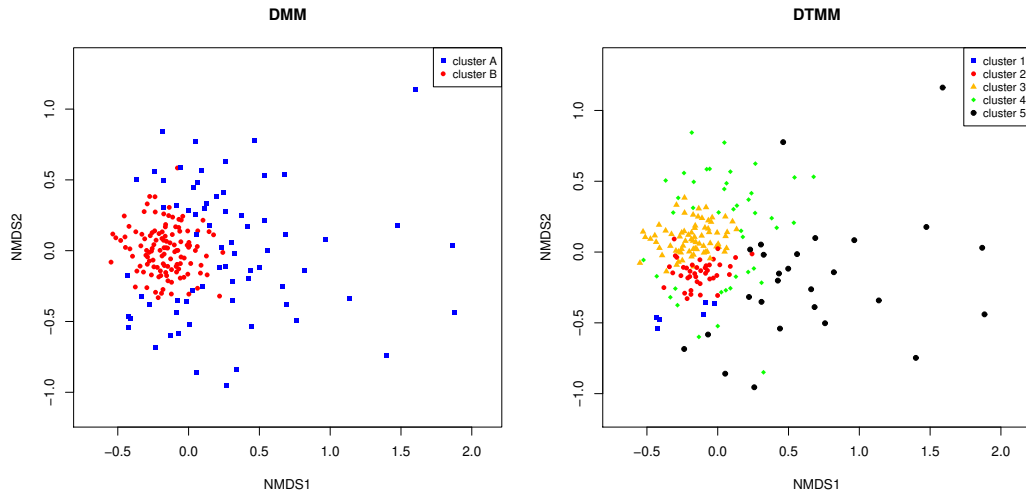


Figure 20: Two-dimensional NMDS plots for the AG IBD dataset. Left: Points are colored and shaped by the resulting cluster given by DMM. Right: Points are colored and shaped based on \mathcal{C}_{LS} .

5 Concluding remarks

We have introduced DTMM as a model-based framework for clustering the amplicon sequencing data in microbiome studies. By directly incorporating the phylogenetic tree, DTMM generalizes the popular DMM in three directions: first, it offers a more flexible covariance structure among different OTUs; second, it provides a way for selecting a subset of internal nodes in the phylogenetic tree that is relevant for clustering; moreover, it replaces the finite mixtures in DMM with Dirichlet process mixtures to allow automatic selection of the number of clusters.

Although the covariance structure offered by DT is richer than that of the Dirichlet distribution, it is still limited compared to the logistic-normal family (LN). In a case with K OTUs, DT models the covariance among OTU counts with $(K - 1)$ dispersion parameters in the series of beta distributions while LN uses $K(K - 1)/2$ parameters in modeling the covariance matrix. It is interesting to further generalize the covariance structure provided by DTMM without making the inference too complicated. When selecting a subset of internal nodes in the phylogenetic tree that are relevant to clustering, DTMM selects a node if it is relevant in identifying *any* cluster. Intuitively, DTMM first selects a subspace in the node space and performs clustering in that space. An alternative direction worth exploring is to allow the nodes selected to be cluster-dependent such that each cluster can deviate from the “mean” cluster at different internal nodes.

Software

For DMM, we use the R package `DirichletMultinomial`. For PAM, we use the `pam` function in the R package `cluster`. For spectral clustering, we use the `specc` function in the R package `kernlab`. For k -means and hierarchical clustering, we use the `kmeans` and `hclust` functions in R. R code for DTMM is freely available at <https://github.com/MaStatLab/DTMM>.

Acknowledgment

LM’s research is partly supported by NSF grants DMS-1749789 and DMS-2013930. Part of this work was completed when JM was supported by a Duke Forge Fellowship.

References

- Aitchison, J. (1982). The statistical analysis of compositional data. *Journal of the Royal Statistical Society: Series B (Methodological)* 44(2), 139–160.
- Anderson, M. J. (2001). A new method for non-parametric multivariate analysis of variance. *Austral ecology* 26(1), 32–46.
- Arumugam, M., J. Raes, E. Pelletier, D. Le Paslier, T. Yamada, D. R. Mende, G. R. Fernandes, J. Tap, T. Bruls, J.-M. Batto, et al. (2011). Enterotypes of the human gut microbiome. *nature* 473(7346), 174.
- Atchison, J. and S. M. Shen (1980). Logistic-normal distributions: Some properties and uses. *Biometrika* 67(2), 261–272.
- Callahan, B. J., P. J. McMurdie, and S. P. Holmes (2017). Exact sequence variants should replace operational taxonomic units in marker-gene data analysis. *The ISME journal* 11(12), 2639.
- Callahan, B. J., P. J. McMurdie, M. J. Rosen, A. W. Han, A. J. A. Johnson, and S. P. Holmes (2016). Dada2: high-resolution sample inference from illumina amplicon data. *Nature methods* 13(7), 581.
- Caporaso, J. G., J. Kuczynski, J. Stombaugh, K. Bittinger, F. D. Bushman, E. K. Costello, N. Fierer, A. G. Pena, J. K. Goodrich, J. I. Gordon, et al. (2010). Qiime allows analysis of high-throughput community sequencing data. *Nature methods* 7(5), 335.
- Costea, P. I., F. Hildebrand, M. Arumugam, F. Bäckhed, M. J. Blaser, F. D. Bushman, W. M. De Vos, S. D. Ehrlich, C. M. Fraser, M. Hattori, et al. (2018). Enterotypes in the landscape of gut microbial community composition. *Nature microbiology* 3(1), 8–16.
- Dahl, D. B. (2006). Model-based clustering for expression data via a dirichlet process mixture model. *Bayesian inference for gene expression and proteomics* 4, 201–218.
- Dennis III, S. Y. (1991). On the hyper-dirichlet type 1 and hyper-liouville distributions. *Communications in Statistics-Theory and Methods* 20(12), 4069–4081.
- Dethlefsen, L. and D. A. Relman (2011). Incomplete recovery and individualized responses of the human distal gut microbiota to repeated antibiotic perturbation. *Proceedings of the National Academy of Sciences* 108(Supplement 1), 4554–4561.

- Ding, T. and P. D. Schloss (2014). Dynamics and associations of microbial community types across the human body. *Nature* 509(7500), 357.
- Escobar, M. D. and M. West (1995). Bayesian density estimation and inference using mixtures. *Journal of the american statistical association* 90(430), 577–588.
- Grice, E. A. and J. A. Segre (2012). The human microbiome: our second genome. *Annual review of genomics and human genetics* 13, 151–170.
- Hoff, P. D. et al. (2006). Model-based subspace clustering. *Bayesian Analysis* 1(2), 321–344.
- Holmes, I., K. Harris, and C. Quince (2012). Dirichlet multinomial mixtures: generative models for microbial metagenomics. *PloS one* 7(2), e30126.
- Ishwaran, H. and L. F. James (2001). Gibbs sampling methods for stick-breaking priors. *Journal of the American Statistical Association* 96(453), 161–173.
- Jaccard, P. (1912). The distribution of the flora in the alpine zone. 1. *New phytologist* 11(2), 37–50.
- Karlsson, F. H., V. Tremaroli, I. Nookaew, G. Bergström, C. J. Behre, B. Fagerberg, J. Nielsen, and F. Bäckhed (2013). Gut metagenome in european women with normal, impaired and diabetic glucose control. *Nature* 498(7452), 99.
- Kaufman, L. and P. J. Rousseeuw (2009). *Finding groups in data: an introduction to cluster analysis*, Volume 344. John Wiley & Sons.
- Knights, D., J. Kuczynski, E. S. Charlson, J. Zaneveld, M. C. Mozer, R. G. Collman, F. D. Bushman, R. Knight, and S. T. Kelley (2011). Bayesian community-wide culture-independent microbial source tracking. *Nature methods* 8(9), 761.
- Koren, O., D. Knights, A. Gonzalez, L. Waldron, N. Segata, R. Knight, C. Huttenhower, and R. E. Ley (2013). A guide to enterotypes across the human body: meta-analysis of microbial community structures in human microbiome datasets. *PLoS computational biology* 9(1), e1002863.
- Kuntz, T. M. and J. A. Gilbert (2017). Introducing the microbiome into precision medicine. *Trends in pharmacological sciences* 38(1), 81–91.
- La Rosa, P. S., J. P. Brooks, E. Deych, E. L. Boone, D. J. Edwards, Q. Wang, E. Sodergren, G. Weinstock, and W. D. Shannon (2012). Hypothesis testing and power calculations for taxonomic-based human microbiome data. *PloS one* 7(12), e52078.
- Lavine, M. et al. (1992). Some aspects of polya tree distributions for statistical modelling. *The annals of statistics* 20(3), 1222–1235.
- Lavine, M. et al. (1994). More aspects of polya tree distributions for statistical modelling. *The Annals of Statistics* 22(3), 1161–1176.
- Li, Z., K. Lee, M. R. Karagas, J. C. Madan, A. G. Hoen, A. J. O’Malley, and H. Li (2018). Conditional regression based on a multivariate zero-inflated logistic-normal model for microbiome relative abundance data. *Statistics in biosciences* 10(3), 587–608.
- Lloyd, S. (1982). Least squares quantization in pcm. *IEEE transactions on information theory* 28(2), 129–137.
- Lozupone, C. and R. Knight (2005). Unifrac: a new phylogenetic method for comparing microbial communities. *Appl. Environ. Microbiol.* 71(12), 8228–8235.
- Mao, J., Y. Chen, and L. Ma (2020). Bayesian graphical compositional regression for micro-

- biome data. *Journal of the American Statistical Association* 115(530), 610–624.
- McDonald, D., A. Birmingham, and R. Knight (2015). Context and the human microbiome. *Microbiome* 3(1), 52.
- McDonald, D., E. Hyde, J. W. Debelius, J. T. Morton, A. Gonzalez, G. Ackermann, A. A. Aksenov, B. Behsaz, C. Brennan, Y. Chen, et al. (2018). American gut: an open platform for citizen science microbiome research. *mSystems* 3(3), e00031–18.
- Miller, J. W. and M. T. Harrison (2013). A simple example of dirichlet process mixture inconsistency for the number of components. In *Advances in neural information processing systems*, pp. 199–206.
- Mosimann, J. E. (1962). On the compound multinomial distribution, the multivariate β -distribution, and correlations among proportions. *Biometrika* 49(1/2), 65–82.
- Neal, R. M. (2000). Markov chain sampling methods for dirichlet process mixture models. *Journal of computational and graphical statistics* 9(2), 249–265.
- Ng, A. Y., M. I. Jordan, and Y. Weiss (2002). On spectral clustering: Analysis and an algorithm. In *Advances in neural information processing systems*, pp. 849–856.
- Qin, J., R. Li, J. Raes, M. Arumugam, K. S. Burgdorf, C. Manichanh, T. Nielsen, N. Pons, F. Levenez, T. Yamada, et al. (2010). A human gut microbial gene catalogue established by metagenomic sequencing. *nature* 464(7285), 59.
- Qin, J., Y. Li, Z. Cai, S. Li, J. Zhu, F. Zhang, S. Liang, W. Zhang, Y. Guan, D. Shen, et al. (2012). A metagenome-wide association study of gut microbiota in type 2 diabetes. *Nature* 490(7418), 55.
- Quince, C., E. E. Lundin, A. N. Andreasson, D. Greco, J. Rafter, N. J. Talley, L. Agreus, A. F. Andersson, L. Engstrand, and M. D’Amato (2013). The impact of crohn’s disease genes on healthy human gut microbiota: a pilot study. *Gut* 62(6), 952–954.
- Scott, J. G. and J. O. Berger (2010). Bayes and empirical-bayes multiplicity adjustment in the variable-selection problem. *The Annals of Statistics*, 2587–2619.
- Sethuraman, J. (1994). A constructive definition of dirichlet priors. *Statistica sinica*, 639–650.
- Silverman, J. D., A. D. Washburne, S. Mukherjee, and L. A. David (2017). A phylogenetic transform enhances analysis of compositional microbiota data. *Elife* 6, e21887.
- Tang, Y., L. Ma, D. L. Nicolae, et al. (2018). A phylogenetic scan test on a dirichlet-tree multinomial model for microbiome data. *The Annals of Applied Statistics* 12(1), 1–26.
- Turnbaugh, P. J., M. Hamady, T. Yatsunenko, B. L. Cantarel, A. Duncan, R. E. Ley, M. L. Sogin, W. J. Jones, B. A. Roe, J. P. Affourtit, et al. (2009). A core gut microbiome in obese and lean twins. *nature* 457(7228), 480.
- Wang, T. and H. Zhao (2017). A dirichlet-tree multinomial regression model for associating dietary nutrients with gut microorganisms. *Biometrics* 73(3), 792–801.
- Wu, G. D., J. Chen, C. Hoffmann, K. Bittinger, Y.-Y. Chen, S. A. Keilbaugh, M. Bewtra, D. Knights, W. A. Walters, R. Knight, et al. (2011). Linking long-term dietary patterns with gut microbial enterotypes. *Science* 334(6052), 105–108.
- Xia, F., J. Chen, W. K. Fung, and H. Li (2013). A logistic normal multinomial regression model for microbiome compositional data analysis. *Biometrics* 69(4), 1053–1063.

Supplementary Materials

A Computational strategies

A.1 Derivation of the Gibbs sampler for DTMM.

Recall that for $\mathbf{Y}_c^I = \{\mathbf{y}_i : c_i = c, i \in I\}$, the marginal likelihood of \mathbf{Y}_c^I at node A given $\gamma(A) = 1$ or $\gamma(A) = 0$ after marginalizing out the sample-specific parameter and the cluster-specific parameter can be written as

$$\begin{aligned} \mathcal{L}_1^A(\mathbf{Y}_c^I) &:= \iint \mathcal{L}^A(\mathbf{Y}_c^I \mid \boldsymbol{\psi}_c^*(A), \gamma(A) = 1, \tilde{\boldsymbol{\psi}}(A)) d\Pi(\boldsymbol{\psi}_c^*(A) \mid \gamma(A) = 1, \tilde{\boldsymbol{\psi}}(A)) \\ &= \iint \prod_{\{i \in I: c_i = c\}} \binom{y_i(A)}{y_i(A_l)} \frac{B(\theta(A)\tau(A) + y_i(A_l), (1 - \theta(A))\tau(A) + y_i(A_r))}{B(\theta(A)\tau(A), (1 - \theta(A))\tau(A))} \\ &\quad \times \frac{\theta(A)^{\theta_0(A)\nu_0(A)-1} (1 - \theta(A))^{(1-\theta_0(A))\nu_0(A)-1}}{B(\theta_0(A)\nu_0(A), (1 - \theta_0(A))\nu_0(A))} d\theta(A) dF^A(\tau), \end{aligned} \quad (\text{S1})$$

$$\begin{aligned} \mathcal{L}_0^A(\mathbf{Y}_c^I \mid \tilde{\boldsymbol{\psi}}(A)) &:= \iint \mathcal{L}^A(\mathbf{Y}_c^I \mid \boldsymbol{\psi}_c^*(A), \gamma(A) = 0, \tilde{\boldsymbol{\psi}}(A)) d\Pi(\boldsymbol{\psi}_c^*(A) \mid \gamma(A) = 0, \tilde{\boldsymbol{\psi}}(A)) \\ &= \prod_{\{i \in I: c_i = c\}} \binom{y_i(A)}{y_i(A_l)} \frac{B(\tilde{\theta}(A)\tilde{\tau}(A) + y_i(A_l), (1 - \tilde{\theta}(A))\tilde{\tau}(A) + y_i(A_r))}{B(\tilde{\theta}(A)\tilde{\tau}(A), (1 - \tilde{\theta}(A))\tilde{\tau}(A))}. \end{aligned} \quad (\text{S2})$$

- (i). **The full conditional of γ .** For each $A \in \mathcal{I}$, let $\mathbf{Y}(A) = \{\mathbf{y}_i(A) : i \in [n]\}$ and $\mathbf{Y}_c(A) = \{\mathbf{y}_i(A) : c_i = c, i \in [n]\}$. We have

$$\begin{aligned} &M_{10}(A \mid \gamma^{-A}, \mathbf{c}, \beta, \lambda) \\ &= \frac{\mathcal{L}(\mathbf{Y} \mid \gamma(A) = 1, \gamma^{-A}, \mathbf{c}, \beta, \lambda)}{\mathcal{L}(\mathbf{Y} \mid \gamma(A) = 0, \gamma^{-A}, \mathbf{c}, \beta, \lambda)} \\ &= \frac{\mathcal{L}(\mathbf{Y}(A_l) \mid \mathbf{Y}(A), \gamma(A) = 1, \mathbf{c}, \beta, \lambda)}{\mathcal{L}(\mathbf{Y}(A_l) \mid \mathbf{Y}(A), \gamma(A) = 0, \mathbf{c}, \beta, \lambda)} \\ &= \frac{\prod_{c \in \mathbf{c}^*} \int \mathcal{L}(\mathbf{Y}_c(A_l) \mid \mathbf{Y}_c(A), \boldsymbol{\psi}_c^*(A), \gamma(A) = 1) d\Pi(\boldsymbol{\psi}_c^*(A) \mid \gamma(A) = 1)}{\int \mathcal{L}(\mathbf{Y}(A_l) \mid \mathbf{Y}(A), \tilde{\boldsymbol{\psi}}(A), \gamma(A) = 0) d\Pi(\tilde{\boldsymbol{\psi}}(A))} \\ &= \frac{\prod_{c \in \mathbf{c}^*} \mathcal{L}_1^A(\mathbf{Y}_c)}{\int \mathcal{L}_0^A(\mathbf{Y} \mid \tilde{\boldsymbol{\psi}}(A)) d\Pi(\tilde{\boldsymbol{\psi}}(A))}. \end{aligned} \quad (\text{S3})$$

(ii). **The full conditional of \mathbf{c} .** For $i \in [n]$, let \mathbf{Y}^{-i} denote the set of samples with sample i excluded and let $\mathbf{c}_{-i}^* = \{\mathbf{c}_{-i}\}$ be the set of distinct values of \mathbf{c}_{-i} . For $c \in \mathbf{c}^*$, we have

$$\begin{aligned}
& \Pr(c_i = c \mid \mathbf{c}_{-i}, \mathbf{Y}, \gamma, \beta, \lambda) \\
& \propto \Pr(c_i = c \mid \mathbf{c}_{-i}, \gamma, \beta, \lambda) \mathcal{L}(\mathbf{y}_i \mid \mathbf{Y}^{-i}, c_i = c, \mathbf{c}_{-i}, \gamma, \beta, \lambda) \\
& \propto n_{-i,c} \times \int \mathcal{L}(\mathbf{y}_i \mid \mathbf{Y}^{-i}, c_i = c, \mathbf{c}_{-i}, \gamma, \beta, \lambda, \tilde{\psi}) d\Pi(\tilde{\psi}) \\
& \propto n_{-i,c} \times \int \left[\int \mathcal{L}(\mathbf{y}_i \mid \mathbf{Y}^{-i}, \psi_c^*, \mathbf{c}_{-i}, \gamma, \beta, \lambda, \tilde{\psi}) d\Pi(\psi_c^* \mid \tilde{\psi}, \gamma) \right] d\Pi(\tilde{\psi}) \\
& \propto n_{-i,c} \times \prod_{\{A \in \mathcal{I}: \gamma(A)=1\}} \frac{\mathcal{L}_1^A(\mathbf{y}_i, \mathbf{Y}_c^{-i})}{\mathcal{L}_1^A(\mathbf{Y}_c^{-i})} \times \left[\int \prod_{\{A \in \mathcal{I}: \gamma(A)=0\}} \frac{\mathcal{L}_0^A(\mathbf{Y} \mid \tilde{\psi}(A))}{\mathcal{L}_0^A(\mathbf{Y}^{-i} \mid \tilde{\psi}(A))} d\Pi(\tilde{\psi}) \right] \\
& \propto n_{-i,c} \times \frac{\mathcal{L}_1(\mathbf{y}_i, \mathbf{Y}_c^{-i} \mid \gamma)}{\mathcal{L}_1(\mathbf{Y}_c^{-i} \mid \gamma)} \times \left[\int \prod_{\{A \in \mathcal{I}: \gamma(A)=0\}} \frac{\mathcal{L}_0^A(\mathbf{Y} \mid \tilde{\psi}(A))}{\mathcal{L}_0^A(\mathbf{Y}^{-i} \mid \tilde{\psi}(A))} d\Pi(\tilde{\psi}) \right], \tag{S4}
\end{aligned}$$

where we use $\mathcal{L}(\mathbf{y}_i \mid -)$ to denote the conditional likelihood of \mathbf{y}_i given certain parameters or other samples. Similarly, we have

$$\begin{aligned}
& \Pr(c_i \neq c_j \text{ for all } j \neq i \mid \mathbf{c}_{-i}, \mathbf{Y}, \gamma, \beta, \lambda) \\
& \propto \Pr(c_i \notin \mathbf{c}_{-i}^* \mid \mathbf{c}_{-i}, \gamma, \beta, \lambda) \mathcal{L}(\mathbf{y}_i \mid \mathbf{Y}^{-i}, c_i \notin \mathbf{c}_{-i}^*, \mathbf{c}_{-i}, \gamma, \beta, \lambda) \\
& \propto \beta \times \int \mathcal{L}(\mathbf{y}_i \mid \mathbf{Y}^{-i}, c_i \notin \mathbf{c}_{-i}^*, \mathbf{c}_{-i}, \gamma, \beta, \lambda, \tilde{\psi}) d\Pi(\tilde{\psi}) \\
& \propto \beta \times \int \left[\int \mathcal{L}(\mathbf{y}_i \mid \mathbf{Y}^{-i}, \psi_{c_i}^*, \mathbf{c}_{-i}, \gamma, \beta, \lambda, \tilde{\psi}) d\Pi(\psi_{c_i}^* \mid \tilde{\psi}, \gamma) \right] d\Pi(\tilde{\psi}) \\
& \propto \beta \times \prod_{\{A \in \mathcal{I}: \gamma(A)=1\}} \mathcal{L}_1^A(\mathbf{y}_i) \times \left[\int \prod_{\{A \in \mathcal{I}: \gamma(A)=0\}} \frac{\mathcal{L}_0^A(\mathbf{Y} \mid \tilde{\psi}(A))}{\mathcal{L}_0^A(\mathbf{Y}^{-i} \mid \tilde{\psi}(A))} d\Pi(\tilde{\psi}) \right] \\
& \propto \beta \times \mathcal{L}_1(\mathbf{y}_i \mid \gamma) \times \left[\int \prod_{\{A \in \mathcal{I}: \gamma(A)=0\}} \frac{\mathcal{L}_0^A(\mathbf{Y} \mid \tilde{\psi}(A))}{\mathcal{L}_0^A(\mathbf{Y}^{-i} \mid \tilde{\psi}(A))} d\Pi(\tilde{\psi}) \right]. \tag{S5}
\end{aligned}$$

Putting together (S4) and (S5), we have

$$\begin{aligned}
\Pr(c_i = c \text{ for some } c \in \mathbf{c}_{-i} \mid \mathbf{c}_{-i}, \mathbf{Y}, \gamma, \beta, \lambda) & \propto n_{-i,c} \times \frac{\mathcal{L}_1(\mathbf{y}_i, \mathbf{Y}_c^{-i} \mid \gamma)}{\mathcal{L}_1(\mathbf{Y}_c^{-i} \mid \gamma)} \\
\Pr(c_i \neq c_j \text{ for all } j \neq i \mid \mathbf{c}_{-i}, \mathbf{Y}, \gamma, \beta, \lambda) & \propto \beta \times \mathcal{L}_1(\mathbf{y}_i \mid \gamma). \tag{S6}
\end{aligned}$$

Note that the integral term in (S4) and (S5) represents the marginal likelihood of \mathbf{y}_i at the nodes with $\gamma(A) = 0$ conditioning on all other samples. This likelihood does not depend on \mathbf{c}_{-i} since the cluster-specific parameters ψ_c^* share the same value at these nodes regardless of c .

A.2 Numerical approximations to the marginal likelihoods

To fully specify the Gibbs sampler, we need to numerically approximate the following marginal likelihoods at $A \in \mathcal{I}$:

1. The marginal likelihoods of a set of samples from the same cluster given $\gamma(A) = 1$: $\mathcal{L}_1^A(\mathbf{Y}_c^I)$;
2. The marginal likelihoods of the samples given $\gamma(A) = 0$:

$$\int \mathcal{L}_0^A(\mathbf{Y} \mid \tilde{\boldsymbol{\psi}}(A)) d\Pi(\tilde{\boldsymbol{\psi}}(A)). \quad (\text{S7})$$

Note that (S7) is a one-dimensional integral that can be easily approximated by quadrature. For $\mathcal{L}_1^A(\mathbf{Y}_c^I)$, let

$$\begin{aligned} g(\theta, \tau) &= \prod_{\{i \in \mathcal{I}: c_i = c\}} \left(\frac{y_i(A)}{y_i(A_l)} \right) \frac{B(\theta\tau + y_i(A_l), (1-\theta)\tau + y_i(A_r))}{B(\theta\tau, (1-\theta)\tau)} \\ h(\theta) &= \frac{\theta^{\theta_0(A)\nu_0(A)-1} (1-\theta)^{(1-\theta_0(A))\nu_0(A)-1}}{B(\theta_0(A)\nu_0(A), (1-\theta_0(A))\nu_0(A))}. \end{aligned} \quad (\text{S8})$$

Then we have

$$\mathcal{L}_1^A(\mathbf{Y}_c^I) = \int \left[\int g(\theta, \tau) dF^A(\tau) \right] h(\theta) d\theta. \quad (\text{S9})$$

Both integrals in (S9) are one-dimensional. In our software, we approximate both integrals with quadratures.

A.3 Sample classification for microbiome data

In this section, we provide details on performing sample classification for microbiome data under the DTMM framework. Let $\tilde{\mathbf{y}}$ be a new microbiome sample from (2.33) in section 2.5. Similar to the computations in (S4), we have

$$\begin{aligned} & \Pr(\tilde{c} = k \mid \tilde{\mathbf{y}}, \mathbf{Y}) \\ & \propto \pi_k \mathcal{L}(\tilde{\mathbf{y}} \mid \tilde{c} = k, \mathbf{Y}) \\ & \propto \pi_k \sum_{\gamma} \pi(\gamma \mid \mathbf{Y}) \iint \mathcal{L}(\tilde{\mathbf{y}} \mid \boldsymbol{\psi}_k^*, \gamma, \tilde{\boldsymbol{\psi}}, \mathbf{Y}_k) d\Pi(\boldsymbol{\psi}_k^* \mid \mathbf{Y}_k, \gamma, \tilde{\boldsymbol{\psi}}) d\Pi(\tilde{\boldsymbol{\psi}} \mid \mathbf{Y}) \\ & \propto \pi_k \sum_{\gamma} \pi(\gamma \mid \mathbf{Y}) \int \left[\int \mathcal{L}(\tilde{\mathbf{y}} \mid \boldsymbol{\psi}_k^*, \gamma, \tilde{\boldsymbol{\psi}}, \mathbf{Y}_k) d\Pi(\boldsymbol{\psi}_k^* \mid \gamma, \tilde{\boldsymbol{\psi}}) \right] d\Pi(\tilde{\boldsymbol{\psi}}) \\ & \propto \pi_k \sum_{\gamma} \pi(\gamma \mid \mathbf{Y}) \prod_{\{A \in \mathcal{I}: \gamma(A)=1\}} \frac{\mathcal{L}_1^A(\tilde{\mathbf{y}}, \mathbf{Y}_k)}{\mathcal{L}_1^A(\mathbf{Y}_k)} \times \left[\int \prod_{\{A \in \mathcal{I}: \gamma(A)=0\}} \frac{\mathcal{L}_0^A(\tilde{\mathbf{y}}, \mathbf{Y} \mid \tilde{\boldsymbol{\psi}}(A))}{\mathcal{L}_0^A(\mathbf{Y} \mid \tilde{\boldsymbol{\psi}}(A))} d\Pi(\tilde{\boldsymbol{\psi}}) \right] \\ & \propto \pi_k \sum_{\gamma} \pi(\gamma \mid \mathbf{Y}) \prod_{\{A \in \mathcal{I}: \gamma(A)=1\}} \frac{\mathcal{L}_1^A(\tilde{\mathbf{y}}, \mathbf{Y}_k)}{\mathcal{L}_1^A(\mathbf{Y}_k)} \times \prod_{\{A \in \mathcal{I}: \gamma(A)=0\}} \int \frac{\mathcal{L}_0^A(\tilde{\mathbf{y}}, \mathbf{Y} \mid \tilde{\boldsymbol{\psi}}(A))}{\mathcal{L}_0^A(\mathbf{Y} \mid \tilde{\boldsymbol{\psi}}(A))} d\Pi(\tilde{\boldsymbol{\psi}}(A)), \end{aligned} \quad (\text{S10})$$

where

$$\begin{aligned} \pi(\boldsymbol{\gamma} \mid \mathbf{Y}) &\propto \pi(\boldsymbol{\gamma}) \mathcal{L}(\mathbf{Y} \mid \boldsymbol{\gamma}) \\ &\propto \pi(\boldsymbol{\gamma}) \prod_{\{A \in \mathcal{I}: \gamma(A)=1\}} \prod_{1 \leq k \leq K} \mathcal{L}_1^A(\mathbf{Y}_k) \times \prod_{\{A \in \mathcal{I}: \gamma(A)=0\}} \int \mathcal{L}_0^A(\mathbf{Y} \mid \tilde{\boldsymbol{\psi}}(A)) d\Pi(\tilde{\boldsymbol{\psi}}(A)). \end{aligned} \quad (\text{S11})$$

Note that (S10) and (S11) can be evaluated numerically.

B Additional materials for the numerical examples

B.1 Logistic normal approximations to the Dirichlet-tree distribution

Lemma 1. For $d \geq 2$ and $d \in \mathbb{N}^+$, let Q be a distribution on \mathbb{S}^{d-1} . Let \mathbb{L}^{d-1} be the set of logistic-normal distributions on \mathbb{S}^{d-1} . We have

$$P = \arg \min_{h \in \mathbb{L}^d} D_{KL}(Q \parallel h),$$

where

$$P \stackrel{d}{=} \text{Logit-Norm}(\tilde{\boldsymbol{\mu}}, \tilde{\boldsymbol{\Sigma}}), \quad \tilde{\boldsymbol{\mu}} = \mathbb{E}_{\mathbf{x} \sim Q} \left[\log \left(\frac{\mathbf{x}_{-d}}{x_d} \right) \right], \quad \tilde{\boldsymbol{\Sigma}} = \mathbb{V}_{\mathbf{x} \sim Q} \left[\log \left(\frac{\mathbf{x}_{-d}}{x_d} \right) \right].$$

Proof. For $h \sim \text{Logit-Norm}(\tilde{\boldsymbol{\mu}}, \tilde{\boldsymbol{\Sigma}}) \in \mathbb{L}^d$, the pdf of h can be written as

$$\begin{aligned} p_h(\mathbf{x}) &= |2\pi\boldsymbol{\Sigma}|^{-\frac{1}{2}} \left(\prod_{j=1}^d x_j \right)^{-1} e^{-\frac{1}{2} \left\{ \log \left(\frac{\mathbf{x}_{-d}}{x_d} \right) - \boldsymbol{\mu} \right\}^\top \boldsymbol{\Sigma}^{-1} \left\{ \log \left(\frac{\mathbf{x}_{-d}}{x_d} \right) - \boldsymbol{\mu} \right\}} \\ &= f(\mathbf{x}) \exp \left\{ \boldsymbol{\eta}^\top \mathbf{T}(\mathbf{x}) - A(\boldsymbol{\eta}) \right\}, \end{aligned}$$

where

$$\begin{aligned} \boldsymbol{\eta} &= \begin{pmatrix} \boldsymbol{\Sigma}^{-1} \boldsymbol{\mu} \\ \text{vec} \left(-\frac{1}{2} \boldsymbol{\Sigma}^{-1} \right) \end{pmatrix} \\ \mathbf{T}(\mathbf{x}) &= \begin{pmatrix} \log \left(\frac{\mathbf{x}_{-d}}{x_d} \right) \\ \text{vec} \left[\log \left(\frac{\mathbf{x}_{-d}}{x_d} \right) \log \left(\frac{\mathbf{x}_{-d}}{x_d} \right)^\top \right] \end{pmatrix} \\ A(\boldsymbol{\eta}) &= \frac{1}{2} \boldsymbol{\mu}^\top \boldsymbol{\Sigma}^{-1} \boldsymbol{\mu} - \frac{1}{2} \log \boldsymbol{\Sigma} \end{aligned}$$

Thus h is an exponential family distribution with natural parameter $\boldsymbol{\eta}$. Note that

$$\begin{aligned} D_{KL}(Q \parallel h) &= \mathbb{E}_Q \left[\log \left(\frac{Q}{h} \right) \right] \\ &= \mathbb{E}_Q [\log Q] + \mathbb{E}_Q [A(\boldsymbol{\eta})] - \mathbb{E}_Q [\boldsymbol{\eta}^\top \mathbf{T}(\mathbf{x})] - \mathbb{E}_Q [\log f(\mathbf{x})] \end{aligned}$$

By the property of the exponential family, we have

$$\nabla_{\boldsymbol{\eta}} D_{\text{KL}}(Q \parallel h) = \mathbb{E}_h[\mathbf{T}(\mathbf{x})] - \mathbb{E}_Q[\mathbf{T}(\mathbf{x})].$$

Let h^* satisfy $\nabla_{\boldsymbol{\eta}} D_{\text{KL}}(Q \parallel h) = 0$, it follows that $\mathbb{E}_{h^*}[\mathbf{T}(\mathbf{x})] = \mathbb{E}_Q[\mathbf{T}(\mathbf{x})]$. Consider the second derivative of $D_{\text{KL}}(Q \parallel h)$ at h^*

$$\nabla \nabla_{\boldsymbol{\eta}} D_{\text{KL}}(Q \parallel h) = \nabla \nabla_{\boldsymbol{\eta}} \mathbb{E}_Q[A(\boldsymbol{\eta})] = \mathbb{V}_{h^*}[\mathbf{T}(\mathbf{x})],$$

which is positive semi-definite. Therefore, h^* minimizes $D_{\text{KL}}(Q \parallel h)$. \square

Therefore, for $Q \stackrel{d}{=} \text{DT}_{\mathcal{T}}(\boldsymbol{\theta}, \boldsymbol{\tau})$, the best approximation to Q in the logistic-normal family is $P \stackrel{d}{=} \text{Logit-Norm}(\tilde{\boldsymbol{\mu}}, \tilde{\boldsymbol{\Sigma}})$ such that

$$\tilde{\boldsymbol{\mu}} = \mathbb{E}_{\mathbf{x} \sim Q} \left[\log \left(\frac{\mathbf{x}_{-d}}{x_d} \right) \right], \quad \tilde{\boldsymbol{\Sigma}} = \mathbb{V}_{\mathbf{x} \sim Q} \left[\log \left(\frac{\mathbf{x}_{-d}}{x_d} \right) \right].$$

For the j -th OTU ω_j , let A_{jp} be its parent in the phylogenetic tree. Let $\alpha_j = \theta(A_{jp})\tau(A_{jp})$ if ω_j is the left child of A_{jp} and $\alpha_j = (1 - \theta(A_{jp}))\tau(A_{jp})$ otherwise. Similarly, for $A \in \mathcal{T}$, let $\beta_A = \theta(A_p)\tau(A_p) - \theta(A)$ if A is the left child of A_p and $\beta_A = (1 - \theta(A_p))\tau(A_p) - \theta(A)$ otherwise. The density function of Q can be written as

$$p_Q(\mathbf{x}) = \left[\prod_{A \in \mathcal{T}} B(\theta(A)\tau(A), (1 - \theta(A))\tau(A)) \right]^{-1} \prod_{j=1}^d x_j^{\alpha_j - 1} \prod_{A \in \mathcal{T}} x_A^{\beta_A},$$

where $x_A = \sum_{j \in A} x_j$. Therefore, the Dirichlet-tree distribution is a member of the exponential family with natural parameter $\boldsymbol{\eta} = \{\{\alpha_j : 1 \leq j \leq d\}, \{\beta_A : A \in \mathcal{T}\}\}$. Let

$$A(\boldsymbol{\eta}) = \sum_{A \in \mathcal{T}} \log [B(\theta(A)\tau(A), (1 - \theta(A))\tau(A))].$$

Again by the property of the exponential family, $\tilde{\boldsymbol{\mu}}$ and $\tilde{\boldsymbol{\Sigma}}$ can be computed with the digamma and the trigamma functions.

B.2 Additional figures for the numerical examples

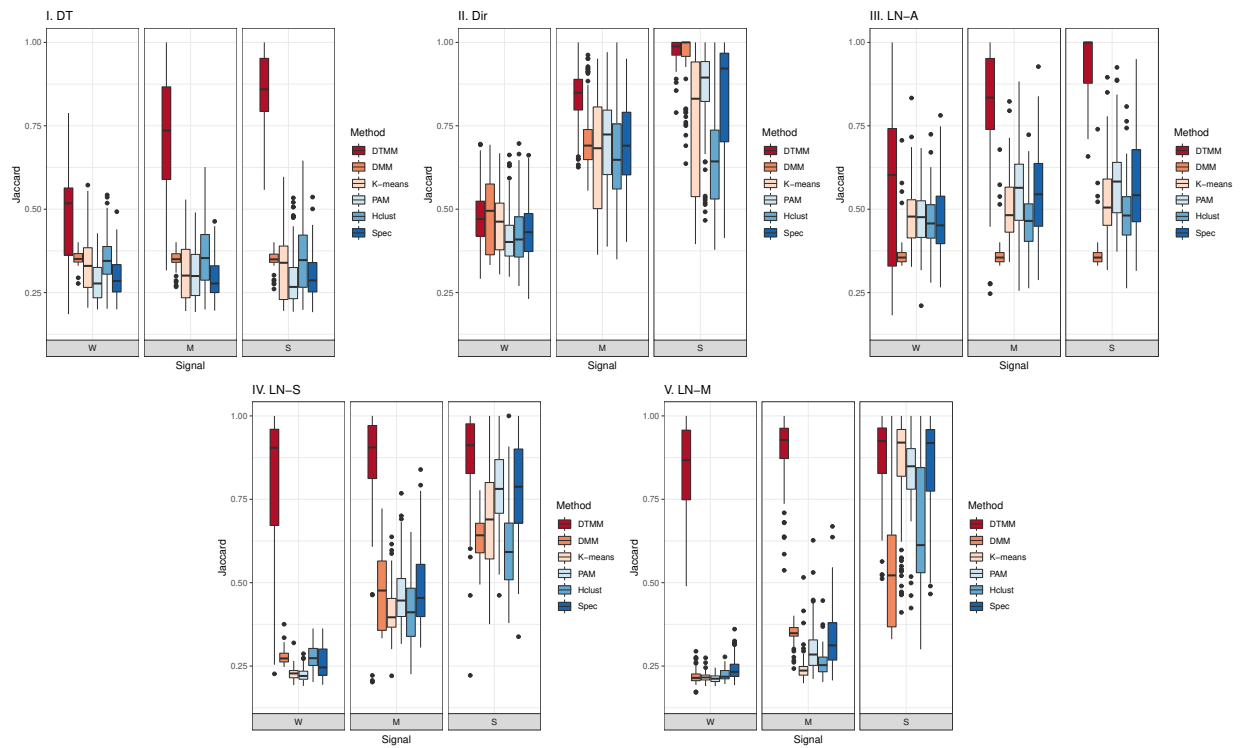


Figure S1: Boxplots of the Jaccard index ($n = 90$).

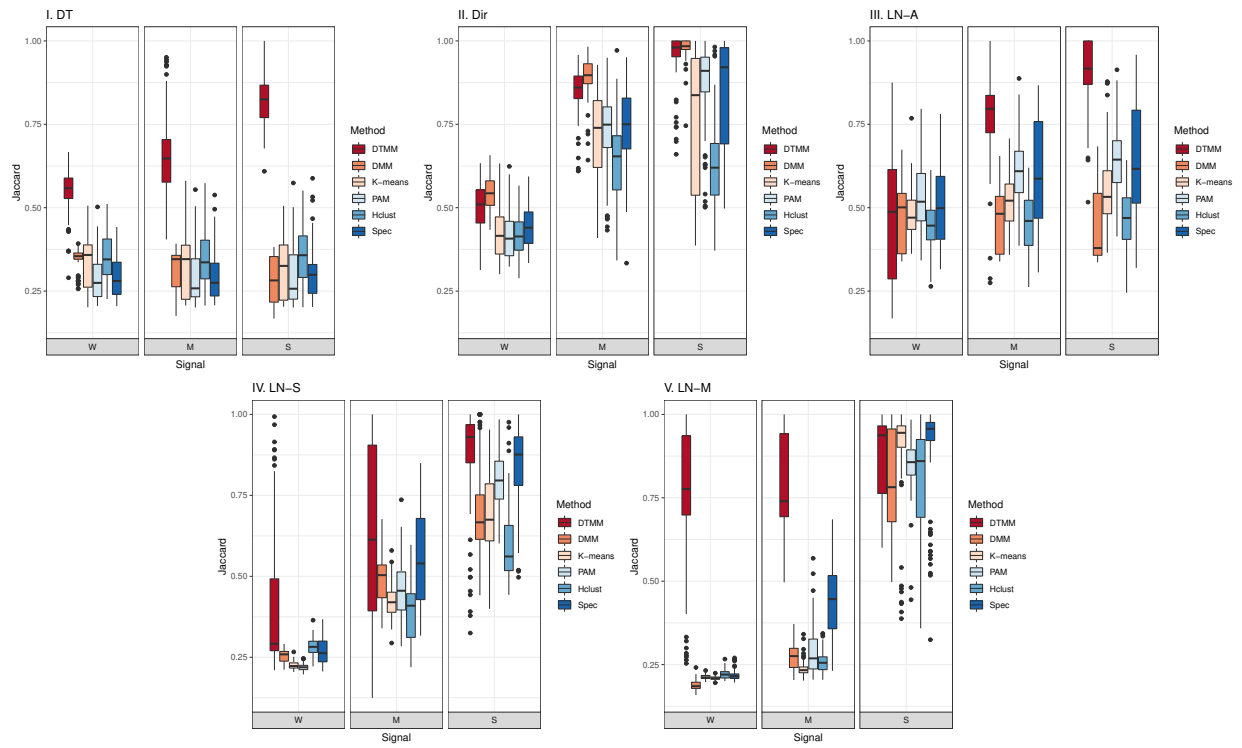


Figure S2: Boxplots of the Jaccard index ($n = 180$).

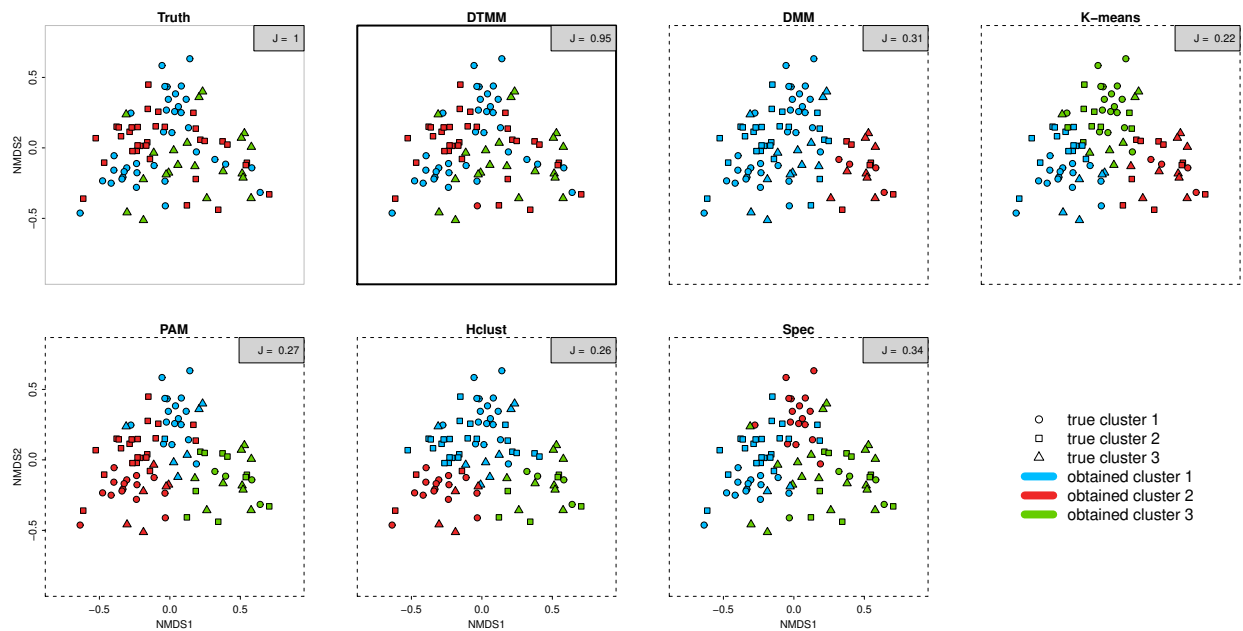


Figure S3: 2D NMDS plot of samples in a simulation round in scenario V ($n = 90$, medium noise level). In each sub-plot, the true clustering is indicated by the shape of the points while the clustering obtained is indicated by the color.

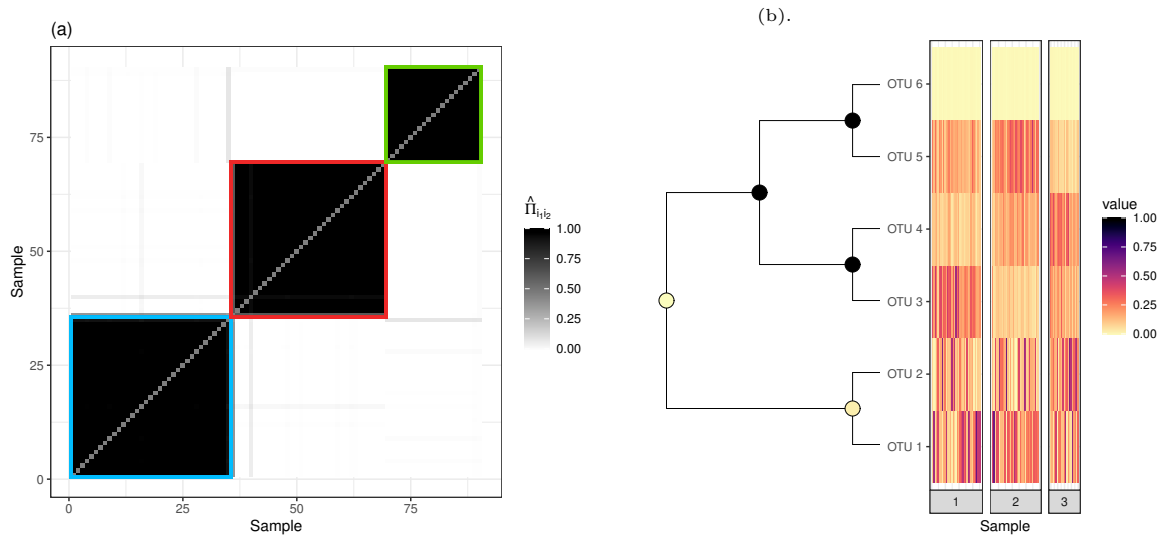


Figure S4: Illustrations for an example from simulation scenario V. (a): Probability of two samples being clustered together by DTMM based on 1000 post-burnin MCMC samples. The samples are ordered by their cluster labels from DTMM. The clusters identified by DTMM are highlighted by squares colored as in Figure 10. (b): An illustration of the node selection property of DTMM. The nodes are colored by their estimated posterior node selection probabilities. The heatmap plots the relative abundance of the samples grouped by their cluster labels from DTMM.

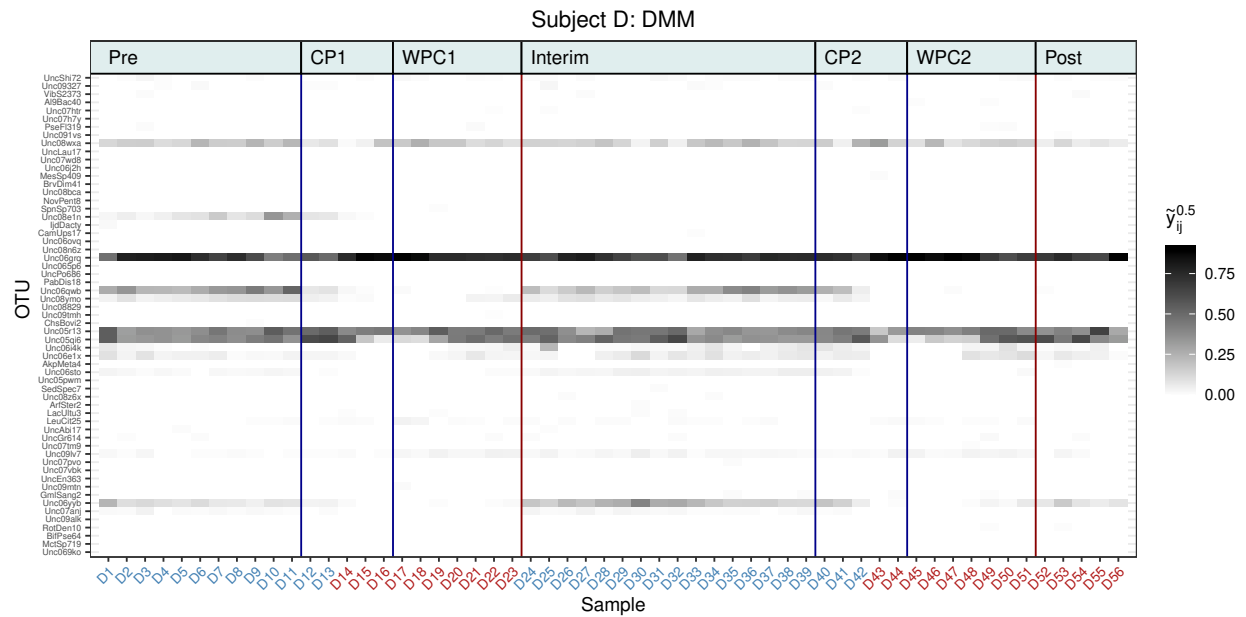


Figure S5: The heatmap of the microbiome samples of patient D (after the square-root transform). Each column represents a specific sample. The columns are ordered by the times the samples were collected. The colors of the x -axis labels represent the clustering labels of the samples returned by DMM. The legends are defined the same way as in [Figure 12](#).

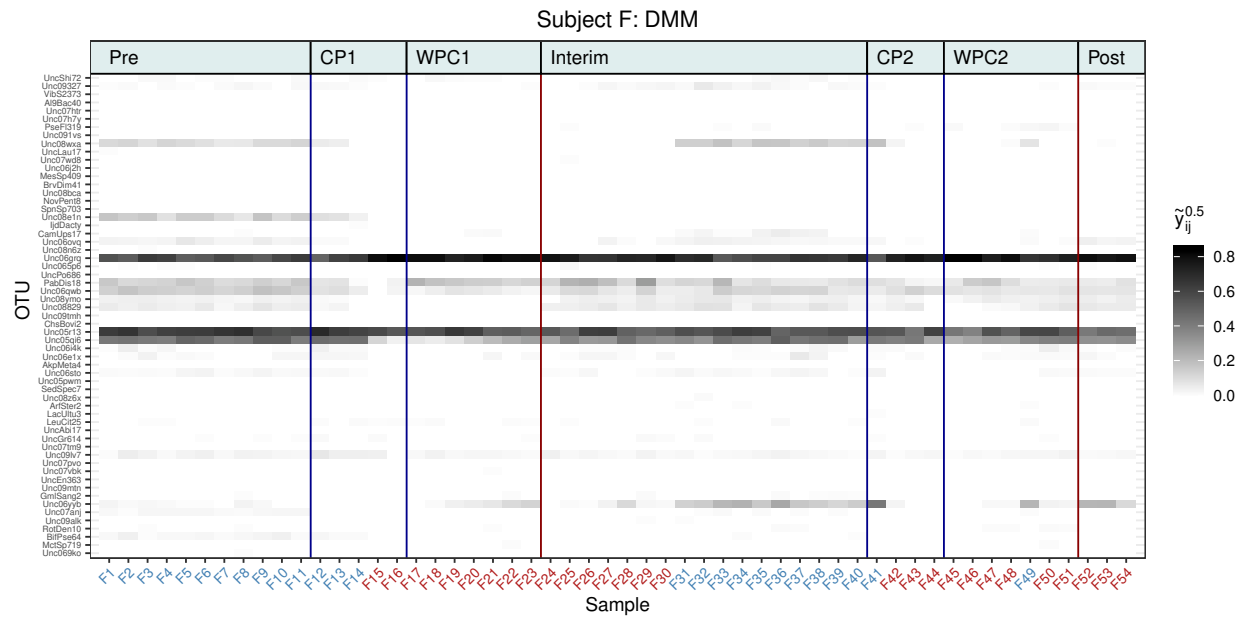


Figure S6: The heatmap of the microbiome samples of patient F (after the square-root transform). Each column represents a specific sample. The columns are ordered by the times the samples were collected. The colors of the x -axis labels represent the clustering labels of the samples returned by DMM. The legends are defined the same way as in [Figure 12](#).

C Additional materials for the applications

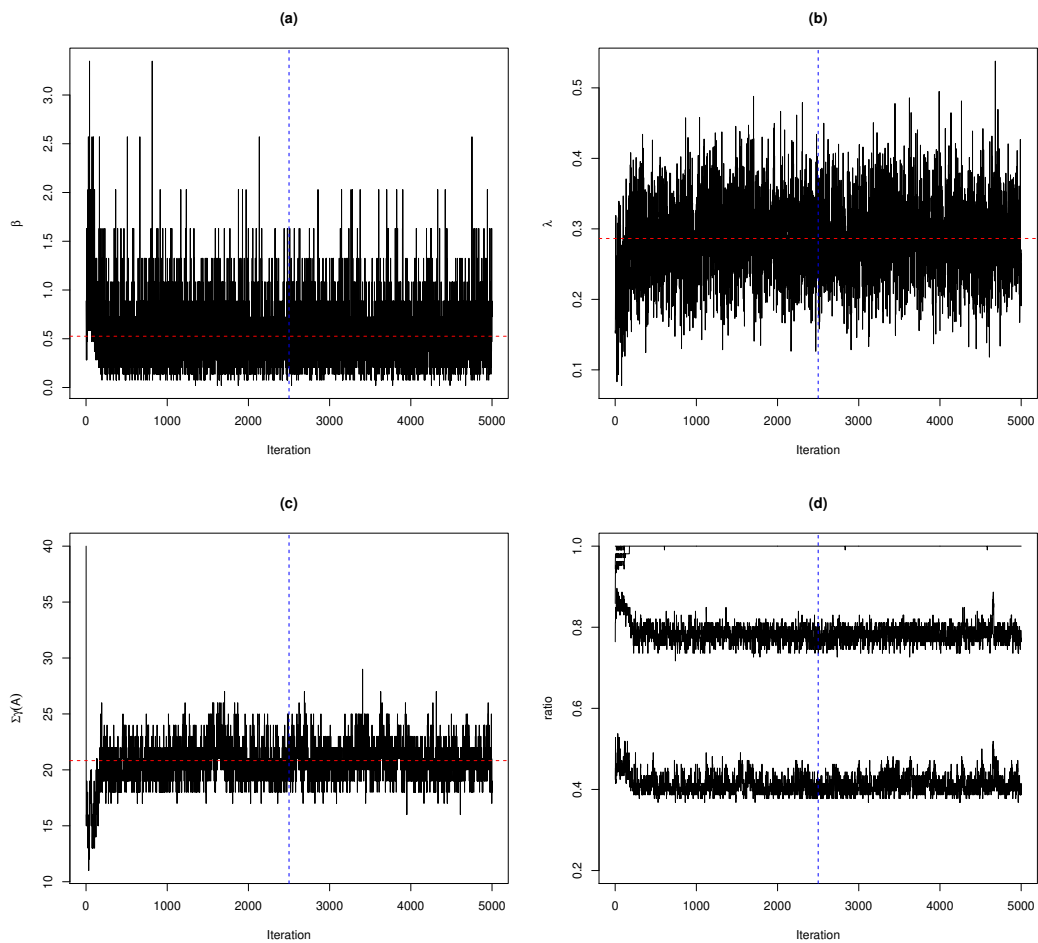


Figure S7: Traceplots of some summary statistics for Section 4.2.

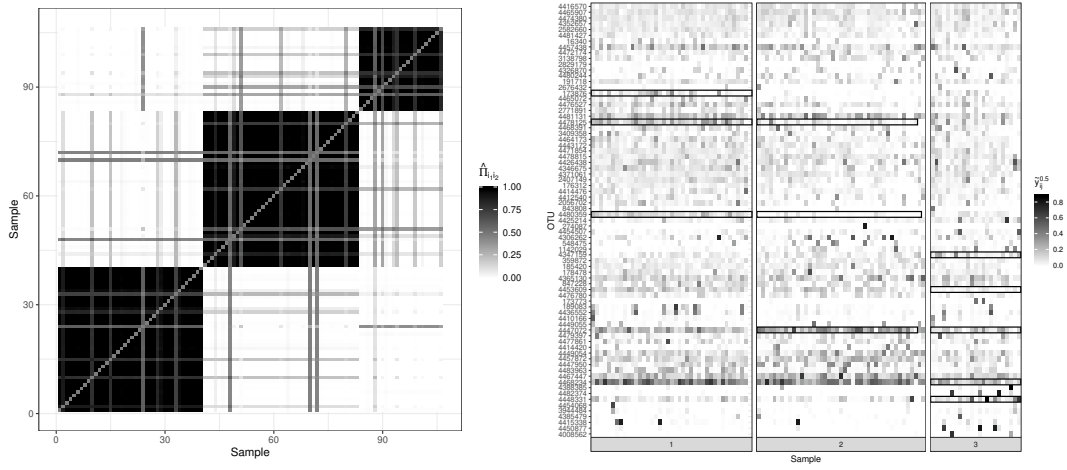


Figure S8: Left: Estimated pairwise co-clustering probabilities. Right: Heatmap of the samples (after the square-root transform) grouped by their labels in \mathcal{C}_{LS} . The black boxes illustrate the characteristic OTUs of each cluster.

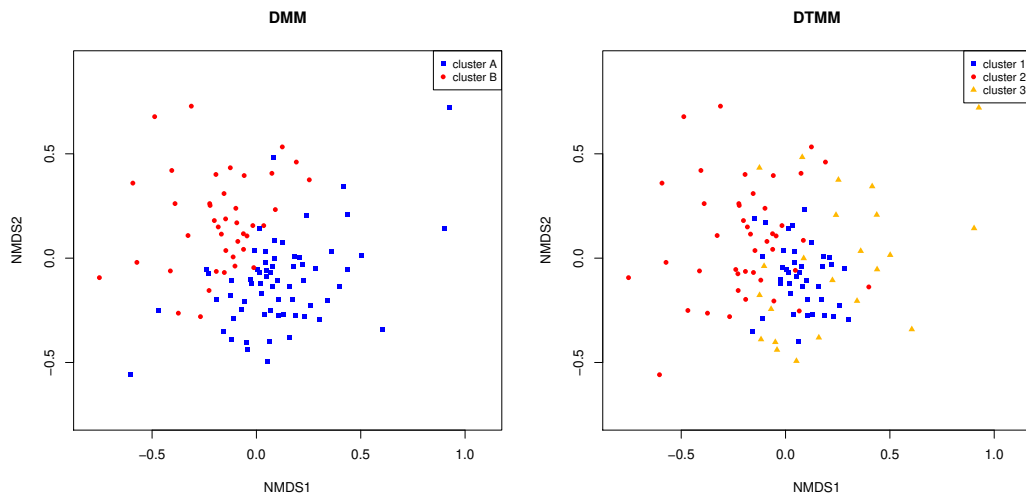


Figure S9: Two-dimensional NMDS plots for the AG diabetes dataset.

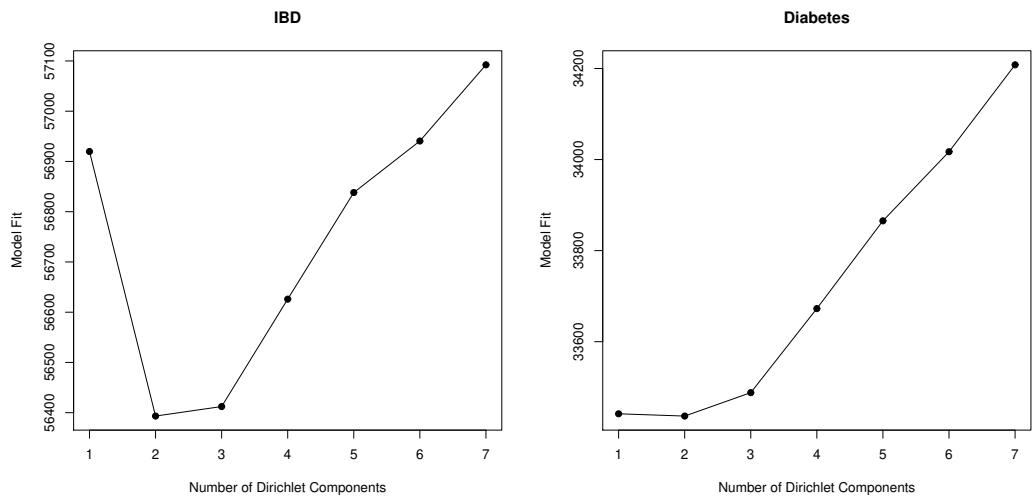


Figure S10: Model fit for DMM with different number of clusters.